12.

I. Clusters and Groups of galaxies

(Reminder: Population synthesis)

II. High redshift galaxies

Clusters and Groups of Galaxies

- Introduction
- The Local group
  - phenomenology
  - mass estimate
  - other components
- Galaxies in clusters and groups
  - the Abell Catalog
  - cD galaxies
  - Morphological classification
  - Spatial distribution: isothermal distribution
  - dynamical mass
- Galaxy groups
- Morphology density relation
- X-ray radiation
  - general properties
  - cooling flows

Schneider, page 223-252

Introduction

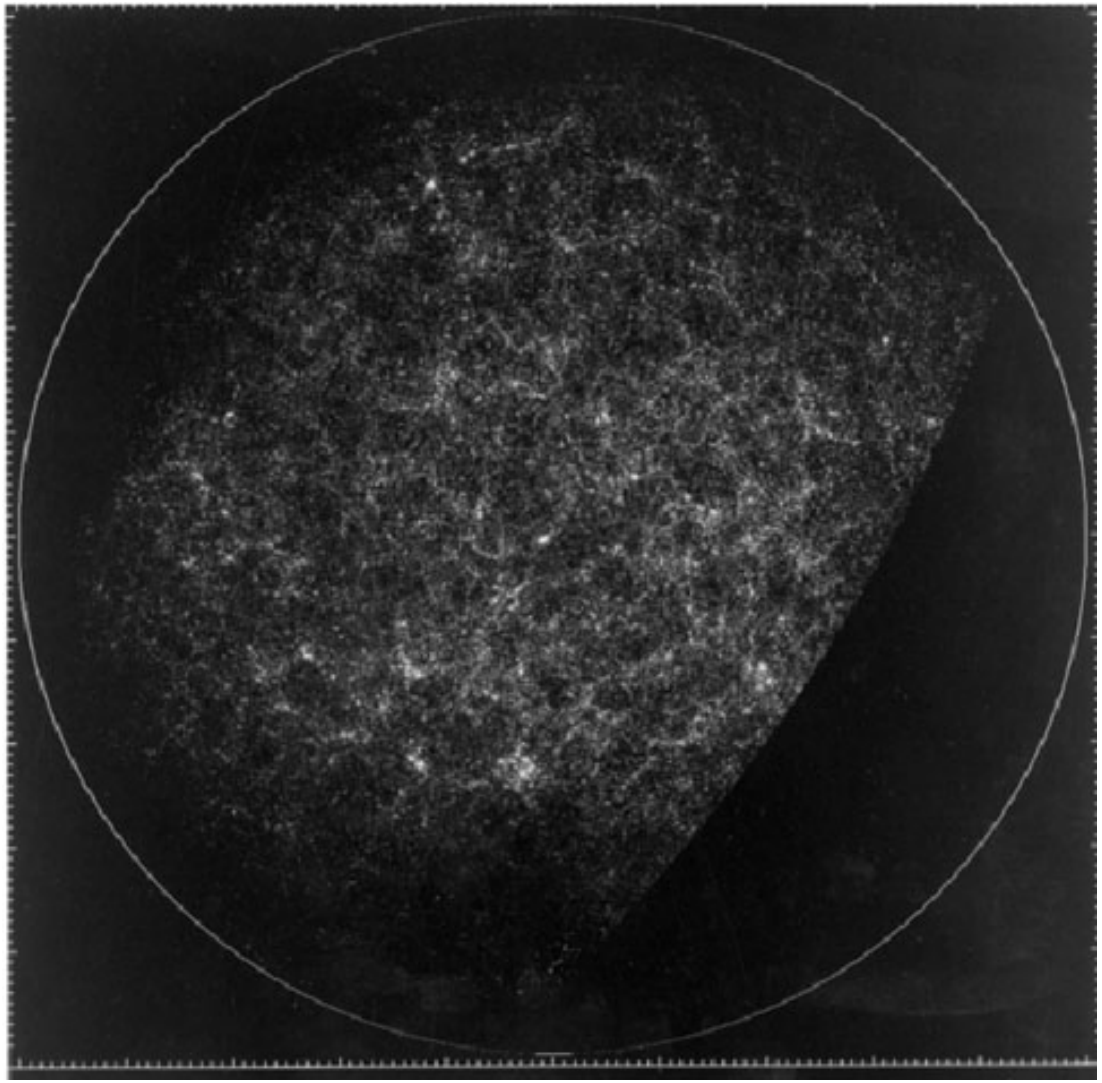

A complete photographic survey of galaxies was made in the Lick Observatory with the 20-inch Carnegie astrograph by Shane & Wirtanen (1967). Galaxy counts were made in cells of size 10' × 10', and the distribution of the number density of galaxies was studied. The general conclusion from this study was that galaxies are mostly located in clusters, the number of galaxies per cluster varying widely from pairs to very rich clusters of the Coma cluster type.http://ned.ipac.caltech.edu/level5/Sept09/Einasto/Einasto5.html

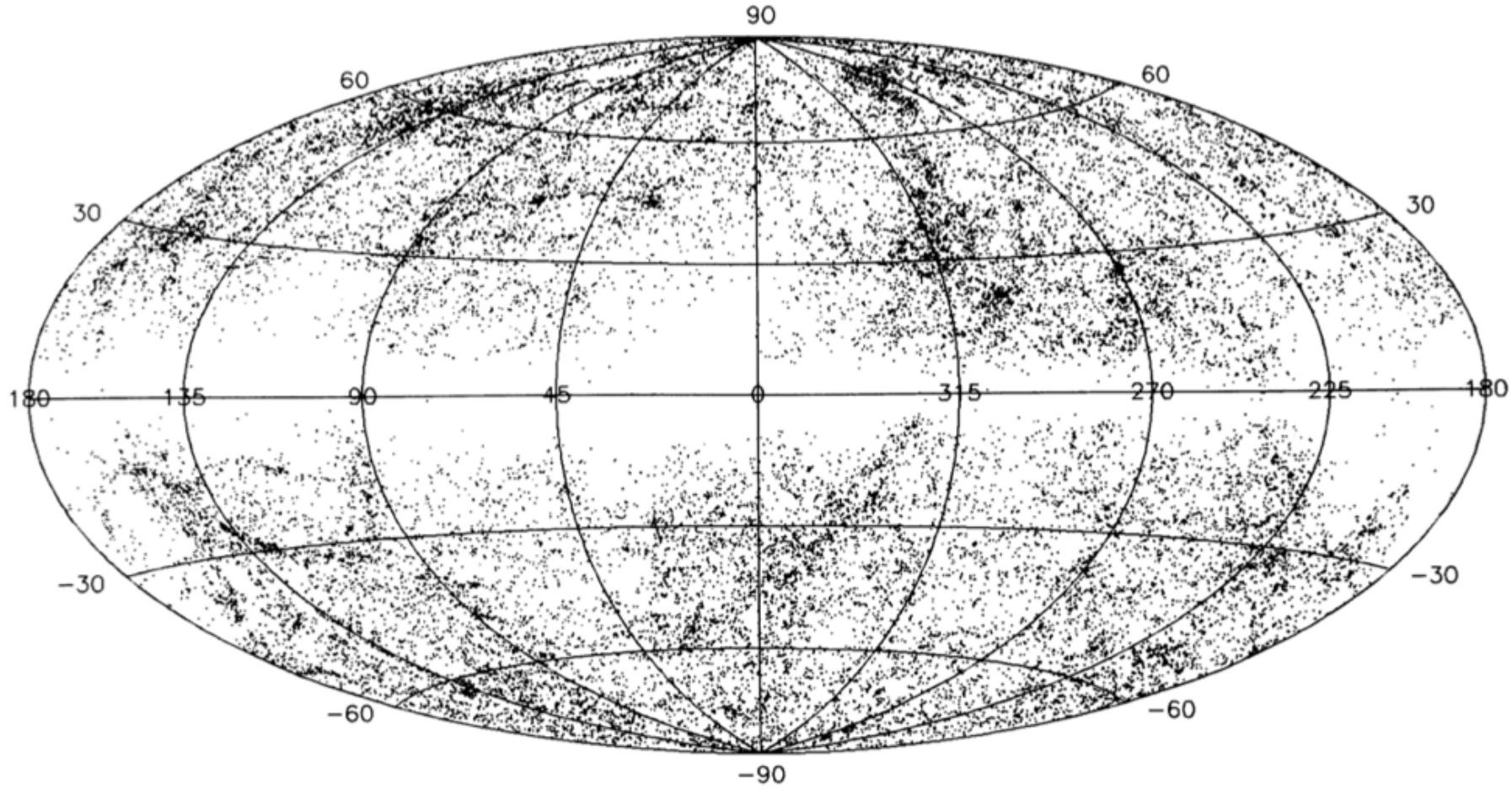
90
60
60
30
30
180
135
90
45
0
315
270
225
180
−30
−30
−60
−60
−90

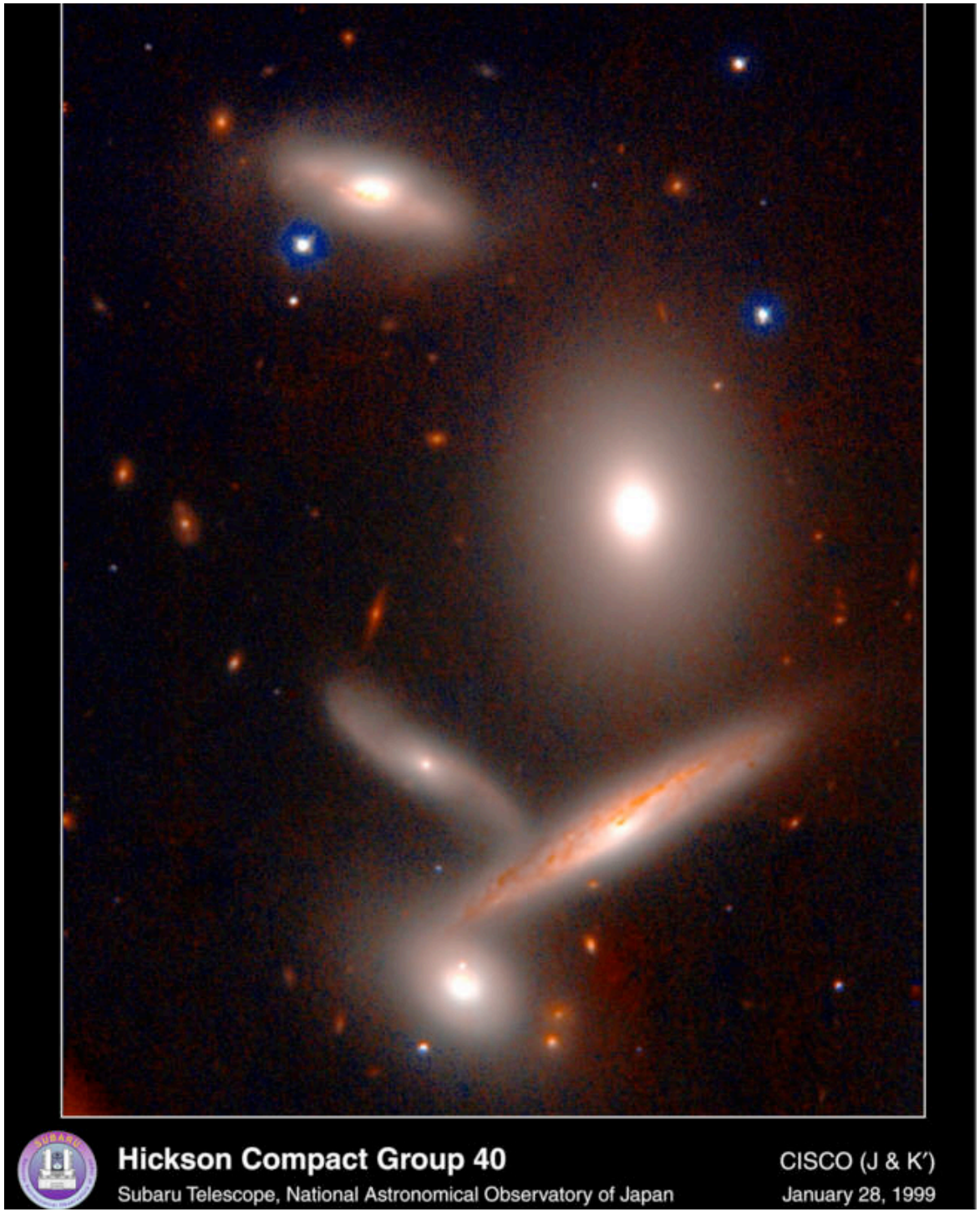
Hickson Compact Group 40
Subaru Telescope, National Astronomical Observatory of Japan
CISCO (J & K′)
January 28, 1999

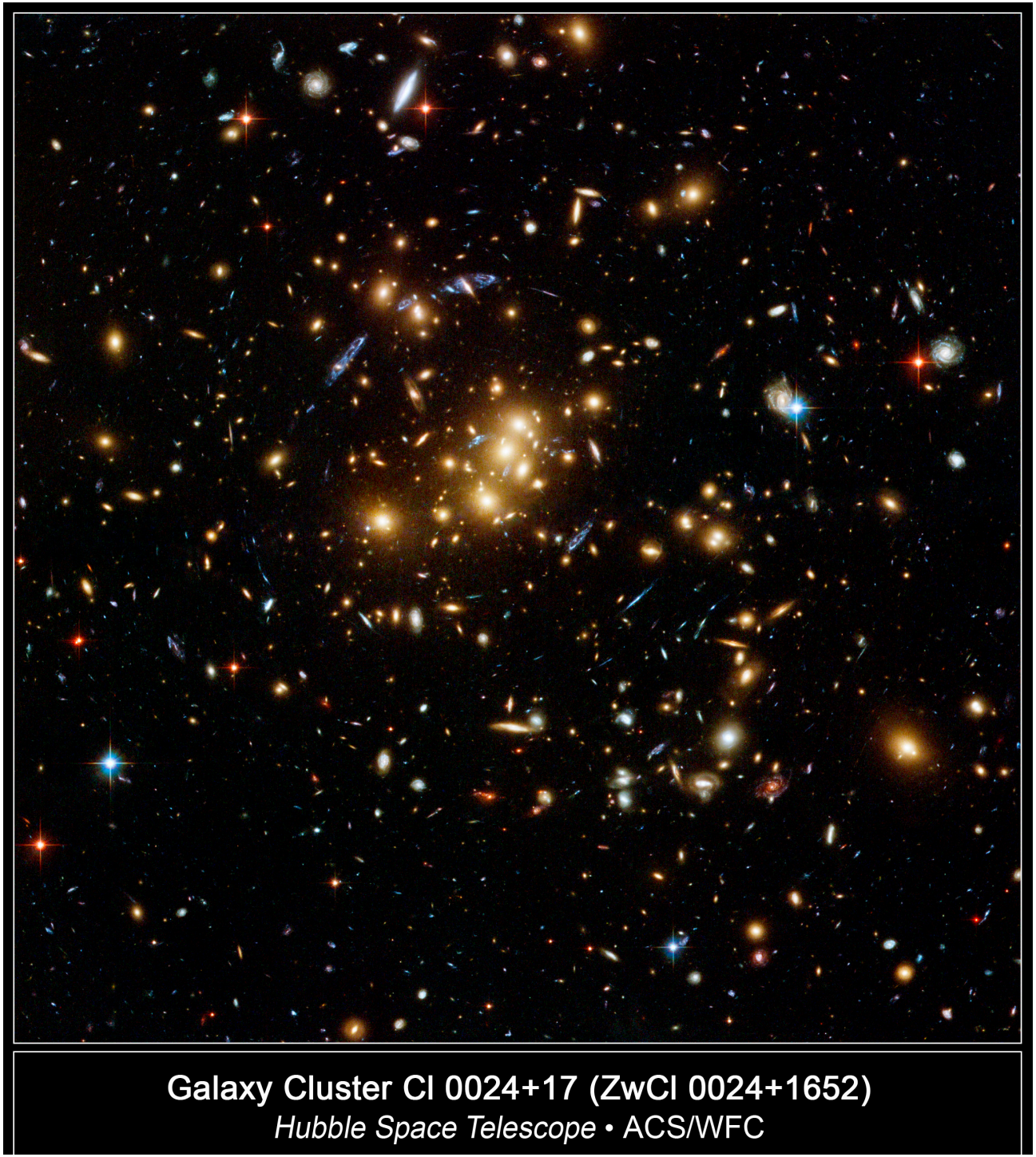

Galaxy Cluster Cl 0024+17 (ZwCl 0024+1652)

Hubble Space Telescope • ACS/WFC

Local group

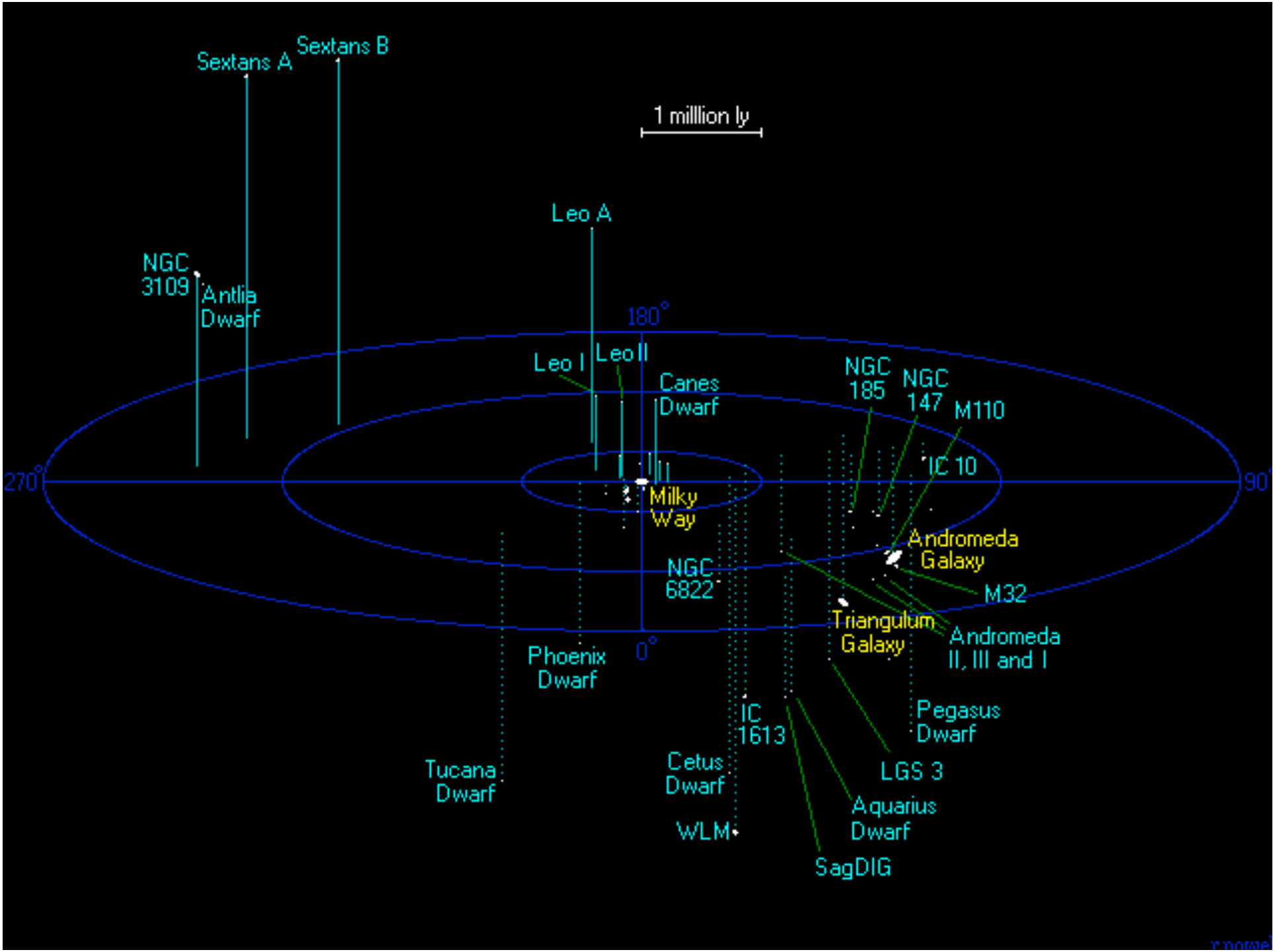
Sextans A
Sextans B
1 milllion ly
Leo A
NGC
3109
Antlia
Dwarf
180°
Leo I
Leo II
Canes
Dwarf
NGC
185
NGC
147
M110
IC 10
270°
90°
Milky
Way
Andromeda
Galaxy
M32
NGC
6822
Triangulum
Galaxy
Andromeda
II, III and I
Phoenix
Dwarf
0°
IC
1613
Pegasus
Dwarf
Tucana
Dwarf
Cetus
Dwarf
LGS 3
Aquarius
Dwarf
WLM
SagDIG

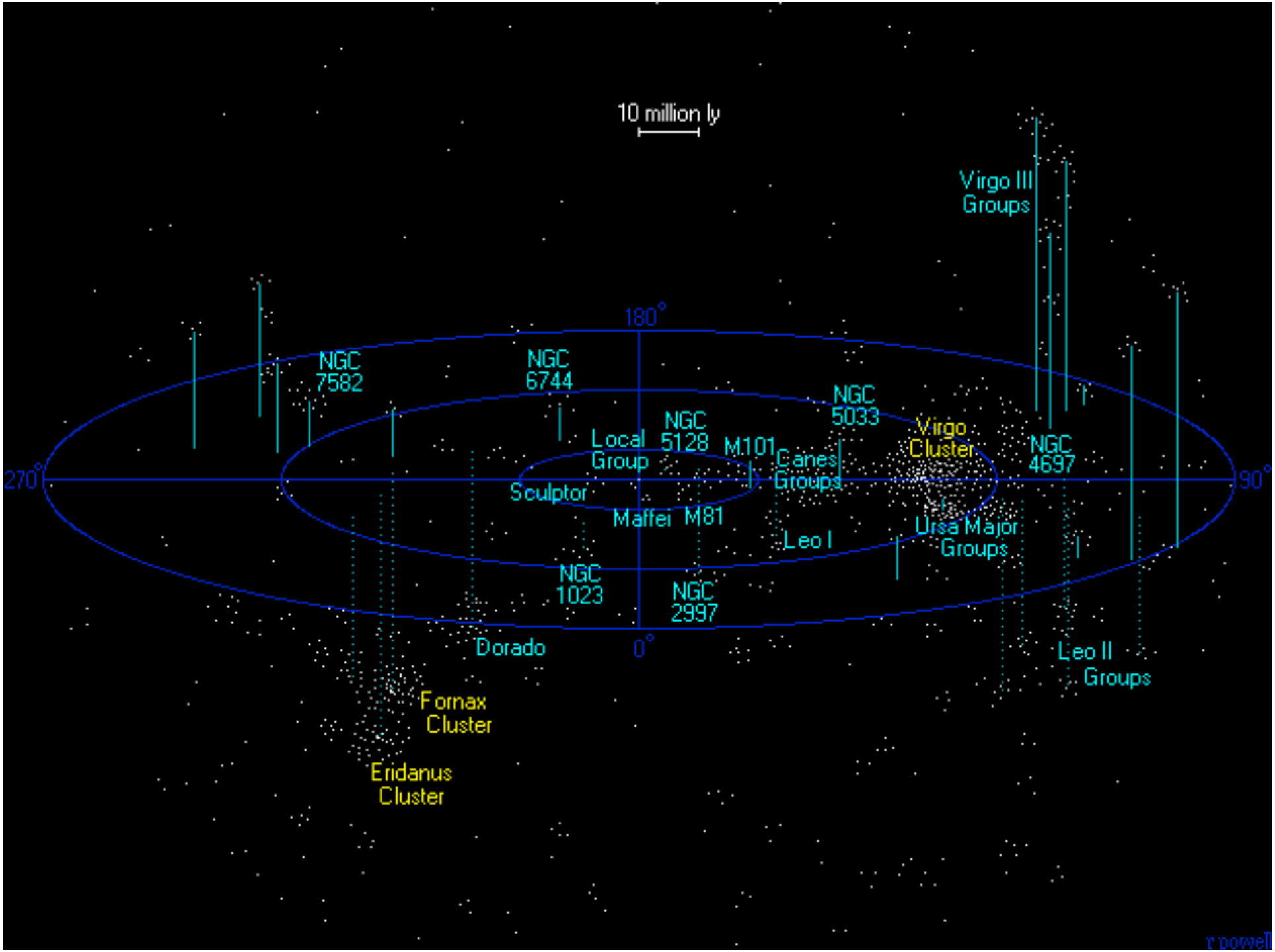
10 million ly
Virgo III
Groups
180°
NGC
7582
NGC
6744
NGC
5033
NGC
5128
Local
Group
M101
Canes
Groups
Virgo
Cluster
NGC
4697
270°
90°
Sculptor
Maffei
M81
Leo I
Ursa Major
Groups
NGC
1023
NGC
2997
0°
Dorado
Leo II
Groups
Fornax
Cluster
Eridanus
Cluster
r powell

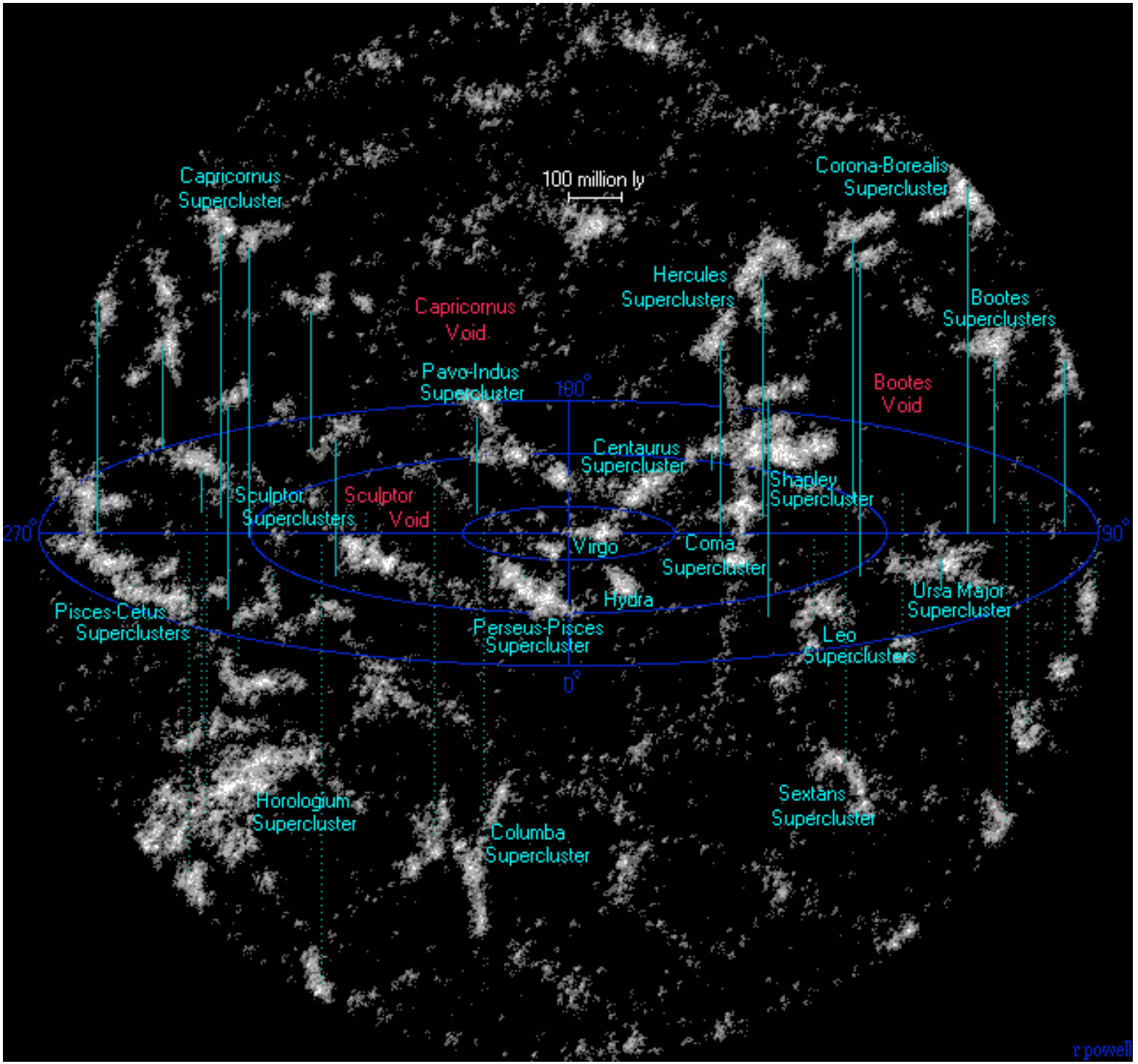
Capricornus
Supercluster
100 million ly
Corona-Borealis
Supercluster
Hercules
Superclusters
Capricornus
Void
Bootes
Superclusters
Pavo-Indus
Supercluster
180°
Bootes
Void
Centaurus
Supercluster
Shapley
Supercluster
Sculptor
Superclusters
Sculptor
Void
270°
90°
Virgo
Coma
Supercluster
Hydra
Ursa Major
Supercluster
Pisces-Cetus
Superclusters
Perseus-Pisces
Supercluster
Leo
Superclusters
0°
Horologium
Supercluster
Columba
Supercluster
Sextans
Supercluster
r powell

- Galaxies in clusters and groups
- Galaxy groups

- Morphology density relation

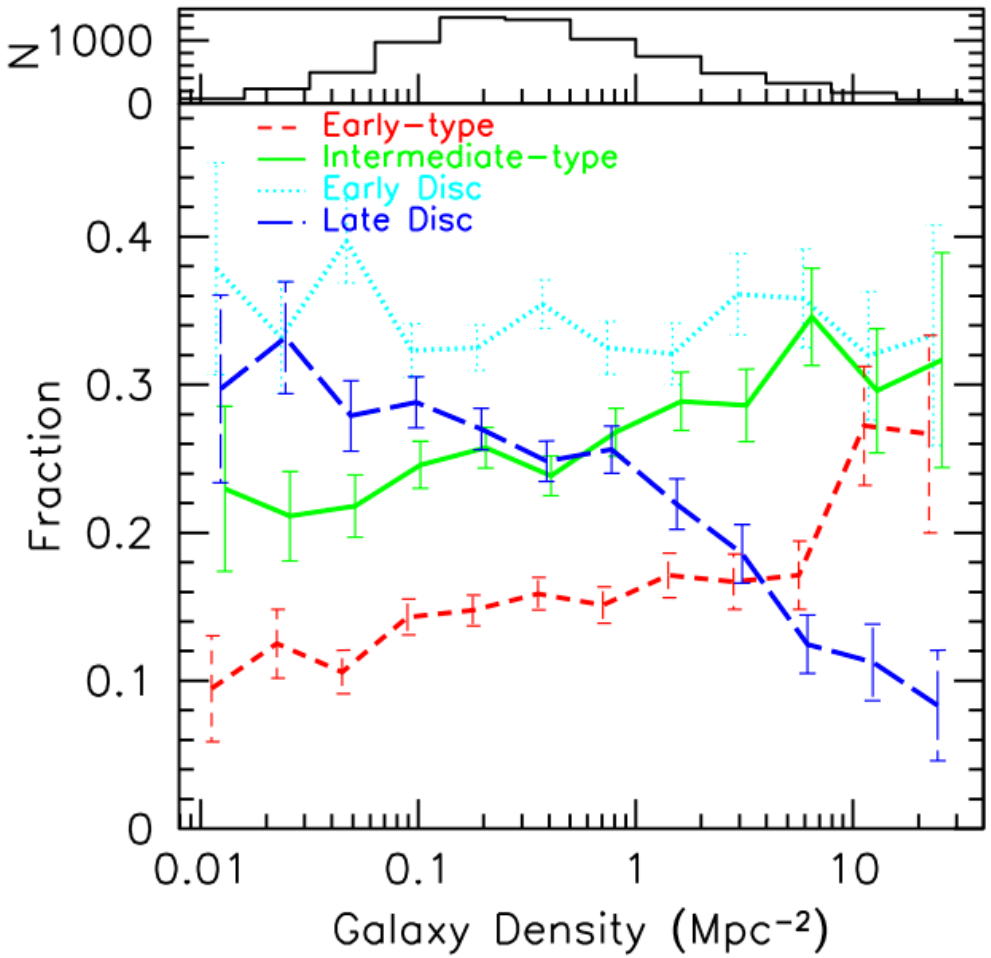

Figure 12. The morphology-density relation for four types of galaxies classified with *Tauto*. The short-dashed, solid, dotted and long-dashed lines represent early-type, intermediate-type, early-disc and late-disc galaxies, respectively. The histogram in the upper panel shows the numbers of galaxies in each bin of local galaxy density.

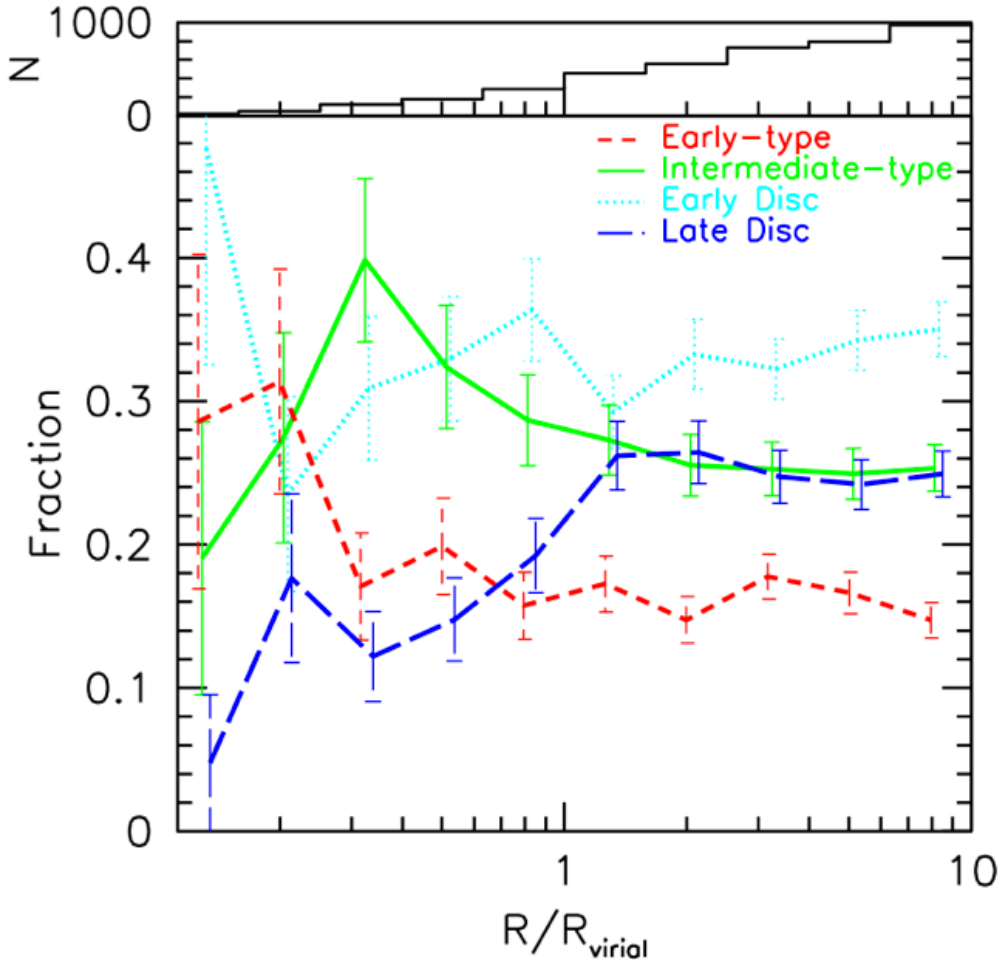

Figure 15. The morphology-radius relation based on *Tauto*. Fractions of each type of a galaxy is plotted against cluster-centric radius to the nearest cluster. The short-dashed, solid, dotted and long-dashed lines represent early-type, intermediate-type, early-disc and late-disc galaxies, respectively. The histogram in the upper panel shows the numbers of galaxies in each bin of cluster-centric radius.

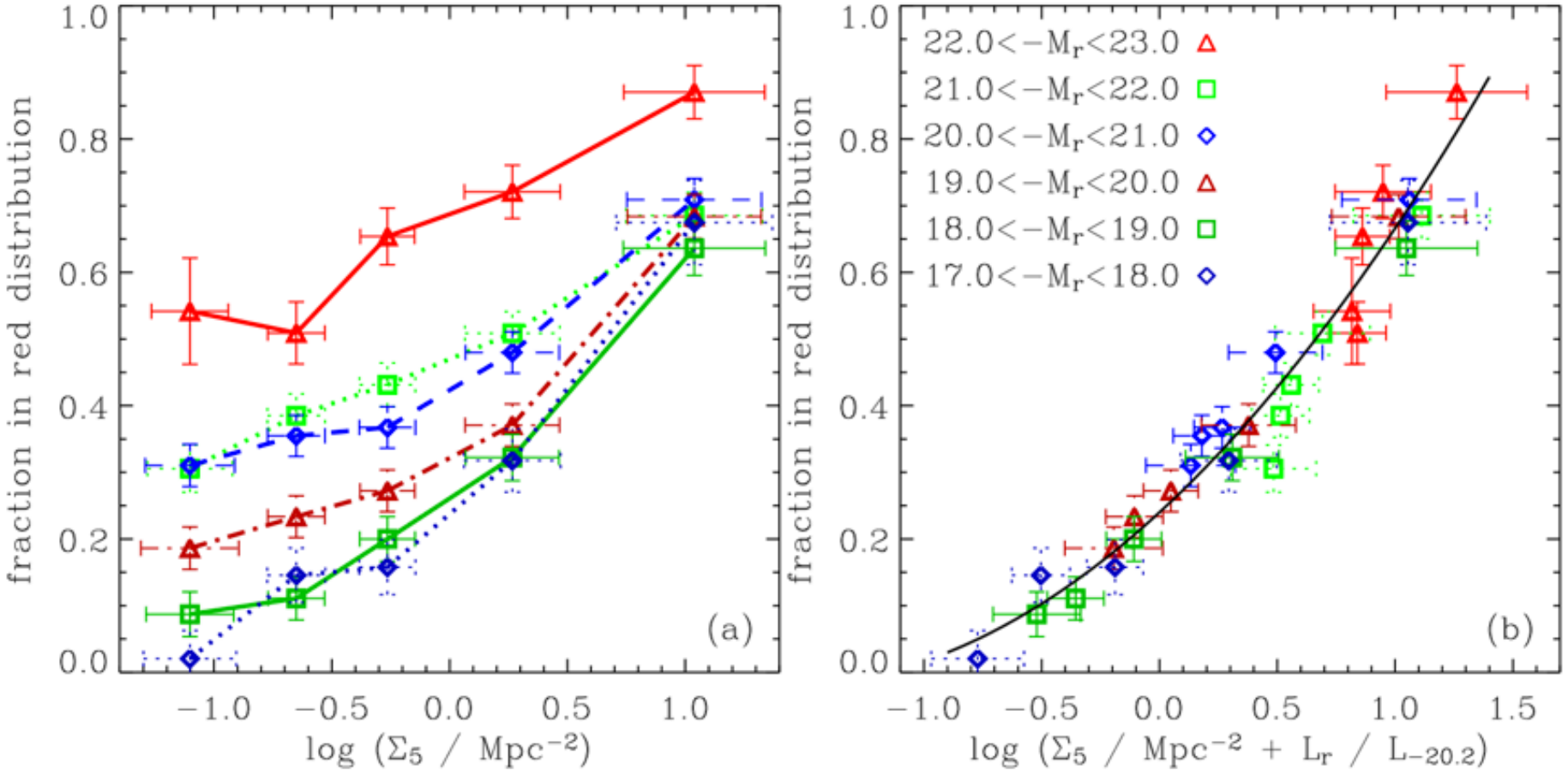

FIGURE 6. The fraction of galaxies in the red distribution as a function of environmental density. Panel (**a**) uses the projected density Σ_5 [same as Fig. 3(a)] while Panel (**b**) uses a combination of the projected density and the *r*-band luminosity (normalized by the luminosity for $M_r = -20.2$). (**b**): The solid line represents a fit to the data points using all luminosity bins.

- X-ray radiation
  - general properties
  - cooling flows

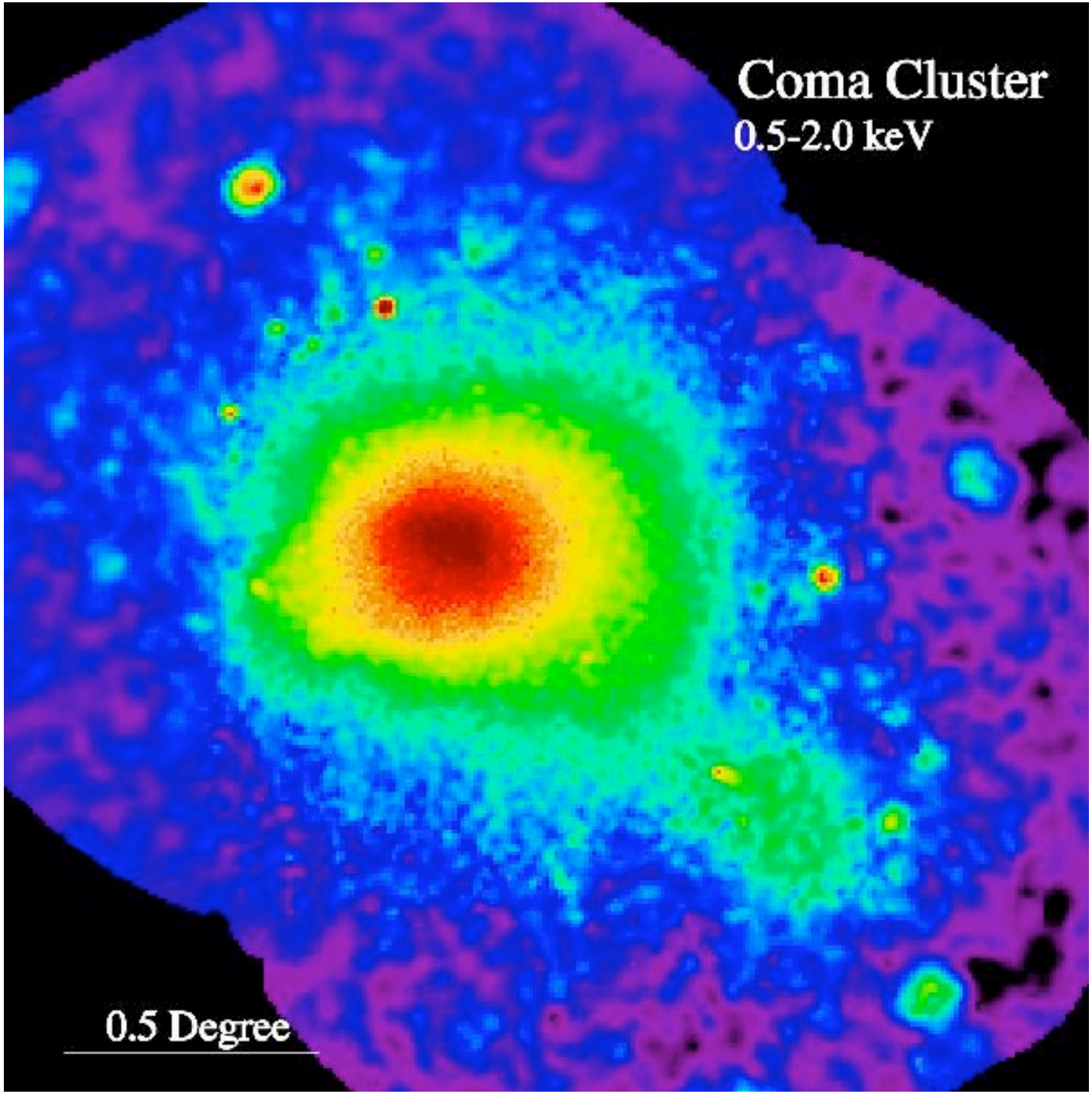
Coma Cluster
0.5-2.0 keV
0.5 Degree

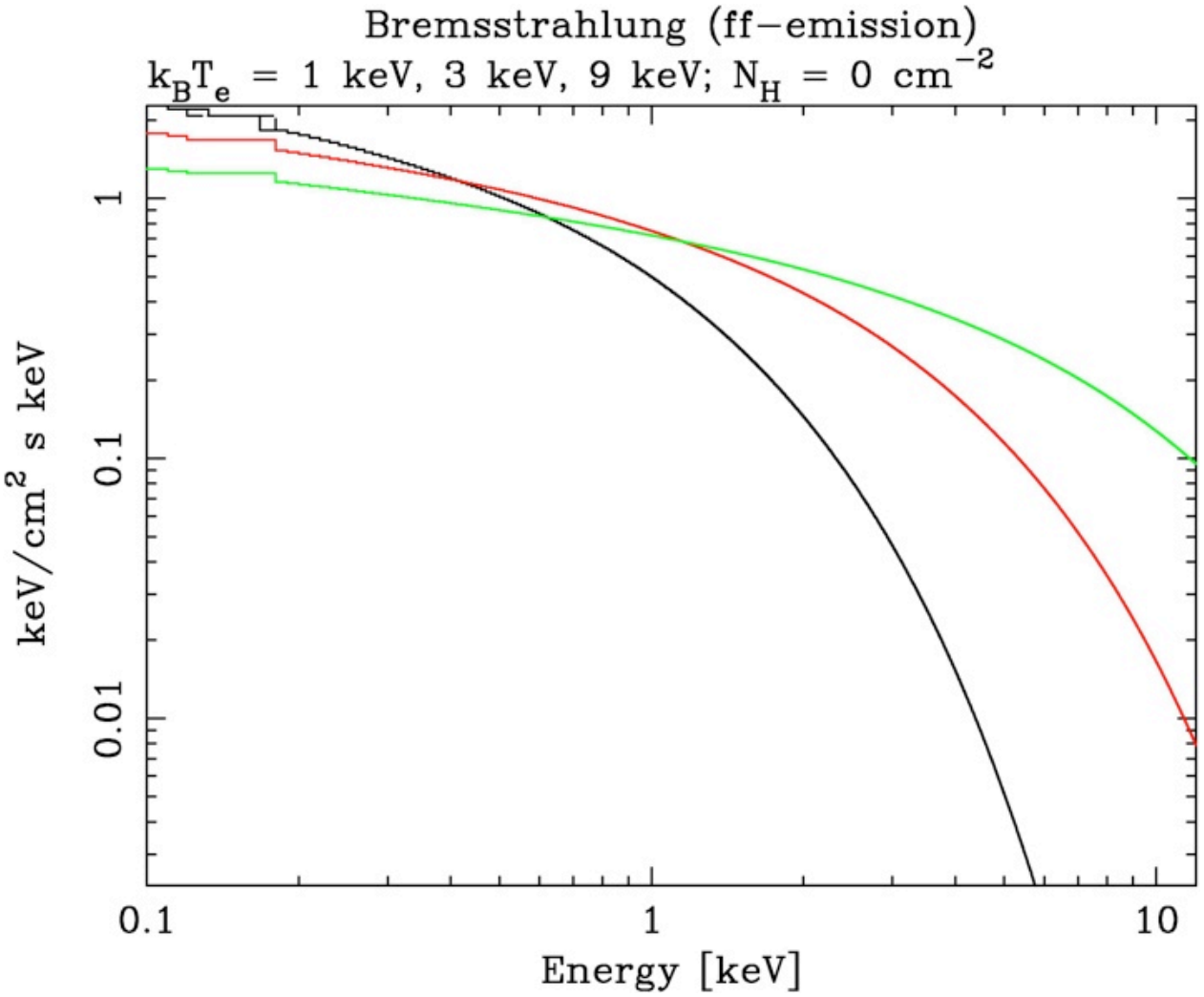
Bremsstrahlung (ff−emission)
$k_B T_e$ = 1 keV, 3 keV, 9 keV; N_H = 0 cm^{-2}
keV/cm^2 s keV
1
0.1
0.01
0.1
1
10
Energy [keV]

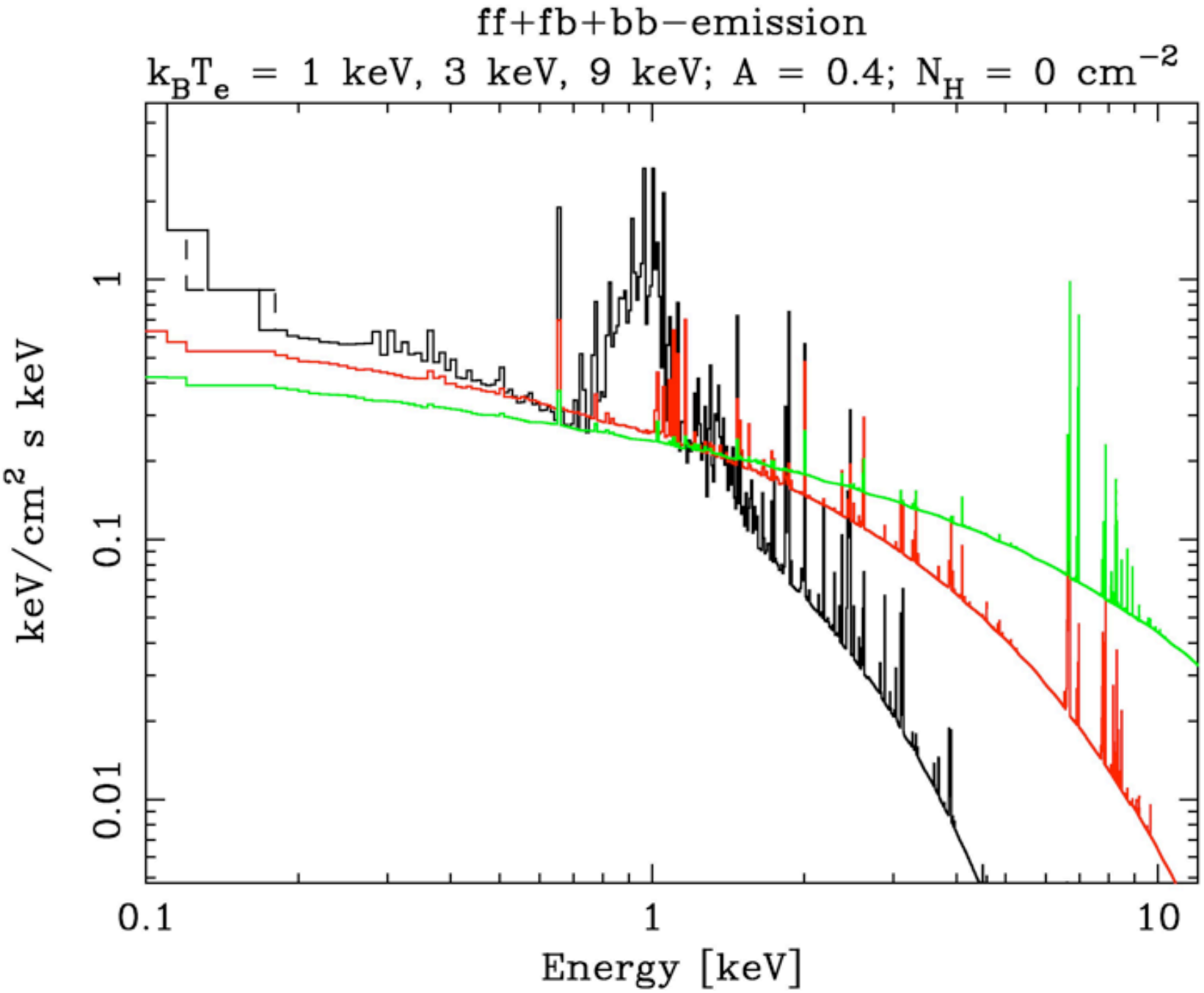
ff+fb+bb−emission
$k_B T_e$ = 1 keV, 3 keV, 9 keV; A = 0.4; N_H = 0 cm^{-2}
keV/cm^2 s keV
1
0.1
0.01
0.1
1
10
Energy [keV]

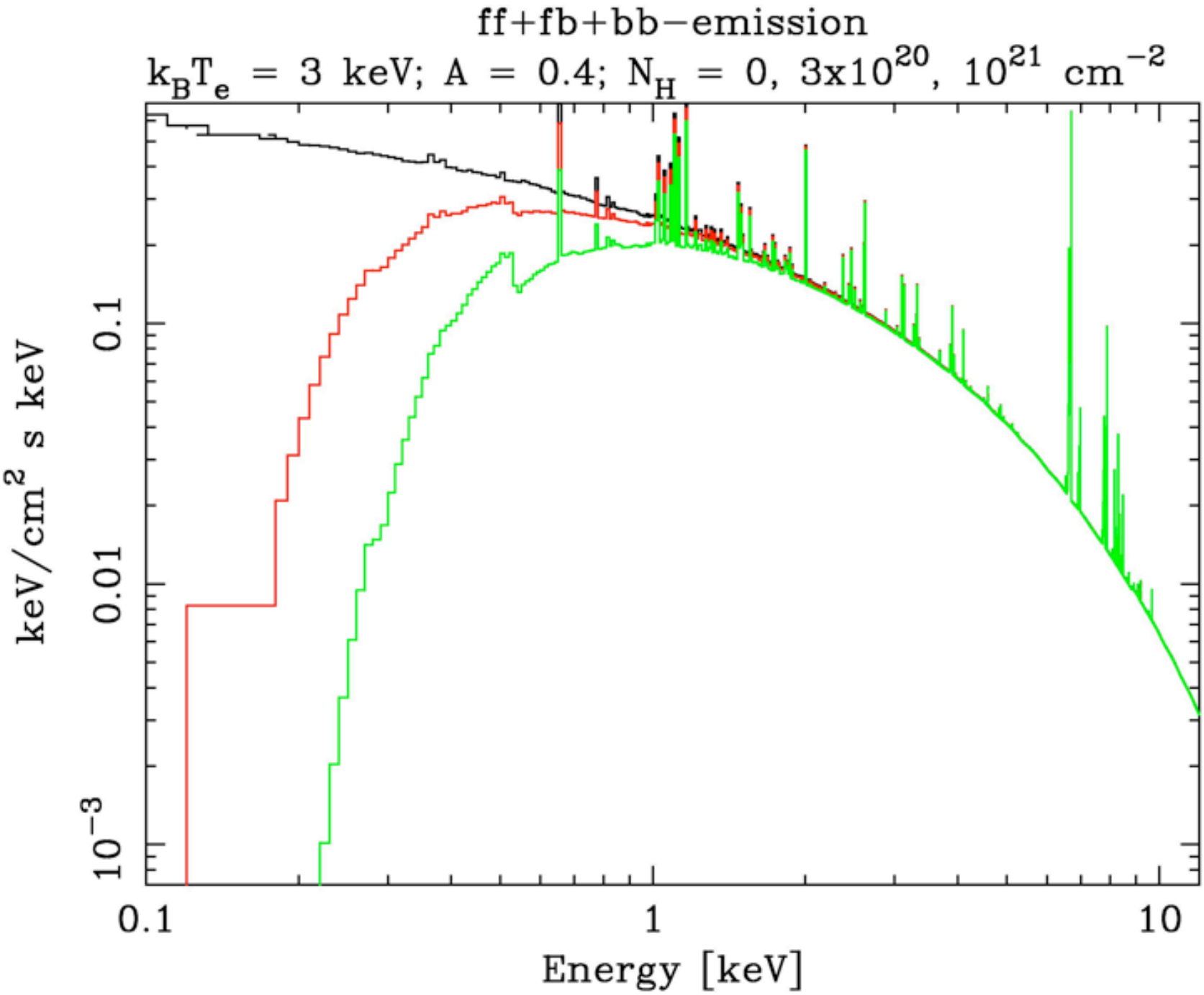
ff+fb+bb−emission
$k_B T_e$ = 3 keV; A = 0.4; N_H = 0, 3x10^{20}, 10^{21} cm^{-2}
keV/cm^2 s keV
10^{-3}
0.01
0.1
0.1
1
10
Energy [keV]

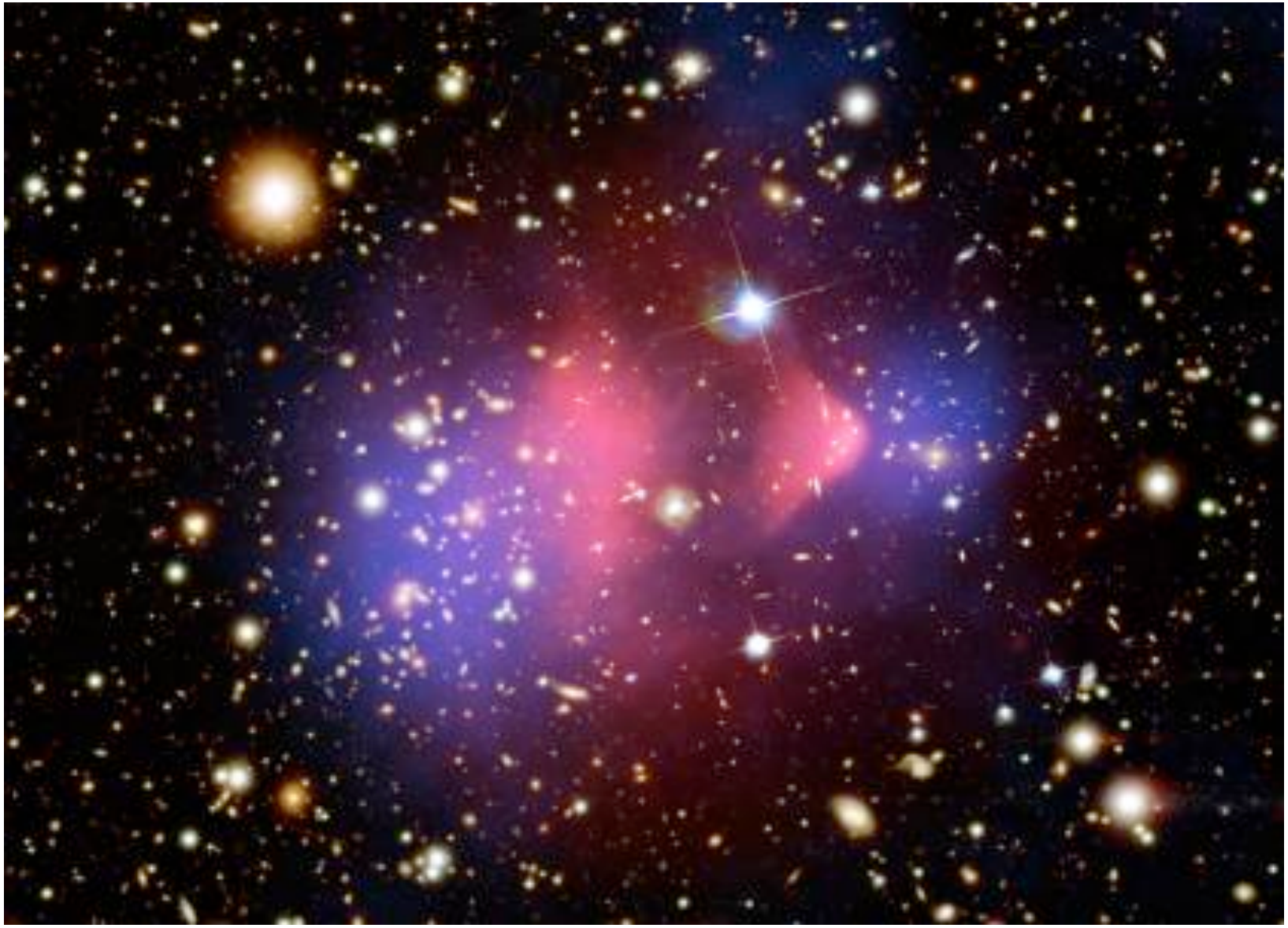

http://chandra.harvard.edu/photo/2006/1e0657/

This composite image shows the galaxy cluster 1E 0657-56, also known as the "bullet cluster."
This cluster was formed after the collision of two large clusters of galaxies, the most energetic event known in the universe since the Big Bang.
Hot gas detected by Chandra in X-rays is seen as two pink clumps in the image and contains most of the "normal," or baryonic, matter in the two clusters. The bullet-shaped clump on the right is the hot gas from one cluster, which passed through the hot gas from the other larger cluster during the collision. An optical image from Magellan and the Hubble Space Telescope shows the galaxies in orange and white. The blue areas in this image show where astronomers find most of the mass in the clusters. The concentration of mass is determined using the effect of so-called gravitational lensing, where light from the distant objects is distorted by intervening matter. Most of the matter in the clusters (blue) is clearly separate from the normal matter (pink), giving direct evidence that nearly all of the matter in the clusters is dark.

The hot gas in each cluster was slowed by a drag force, similar to air resistance, during the collision. In contrast, the dark matter was not slowed by the impact because it does not interact directly with itself or the gas except through gravity. Therefore, during the collision the dark matter clumps from the two clusters moved ahead of the hot gas, producing the separation of the dark and normal matter seen in the image. If hot gas was the most massive component in the clusters, as proposed by alternative theories of gravity, such an effect would not be seen. Instead, this result shows that dark matter is required.

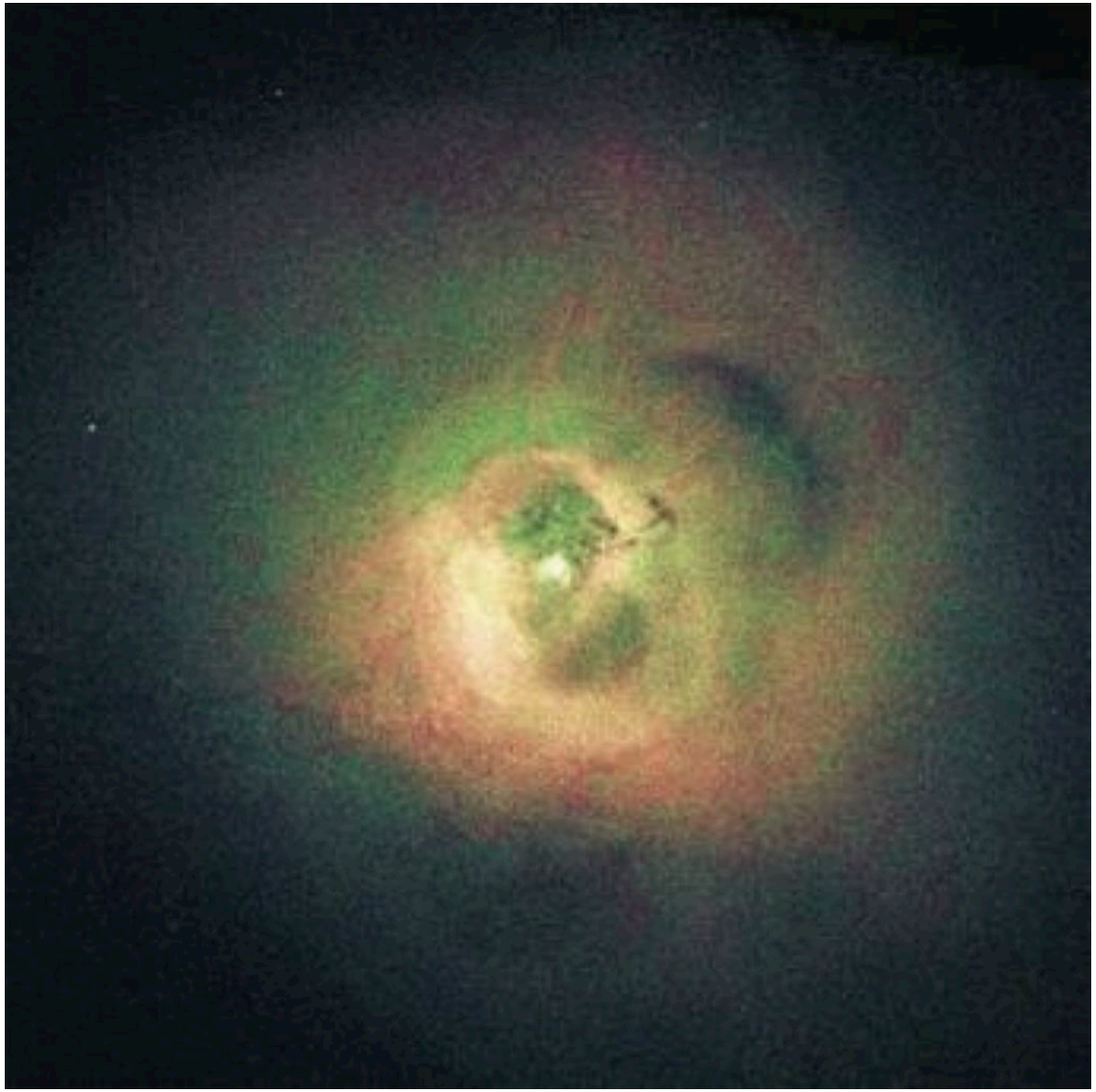

- Chandra X-ray image of the cluster Perseus-A (Fabian et al. 2003, MNRAS, 344, L43). The central galaxy in this cluster, NGC 1275, is a radio source blowing radio "bubbles" into the intracluster medium. The image is 5.8' on a side. The Constellation-X field of view is quite important for this science, combined with ~ 5" HPD PSF.
- http://constellation.gsfc.nasa.gov/old_conx_pages/resources/townhall_2006/booklet_images/ch4.html

Reminder: Population synthesis

Stellar spectra I

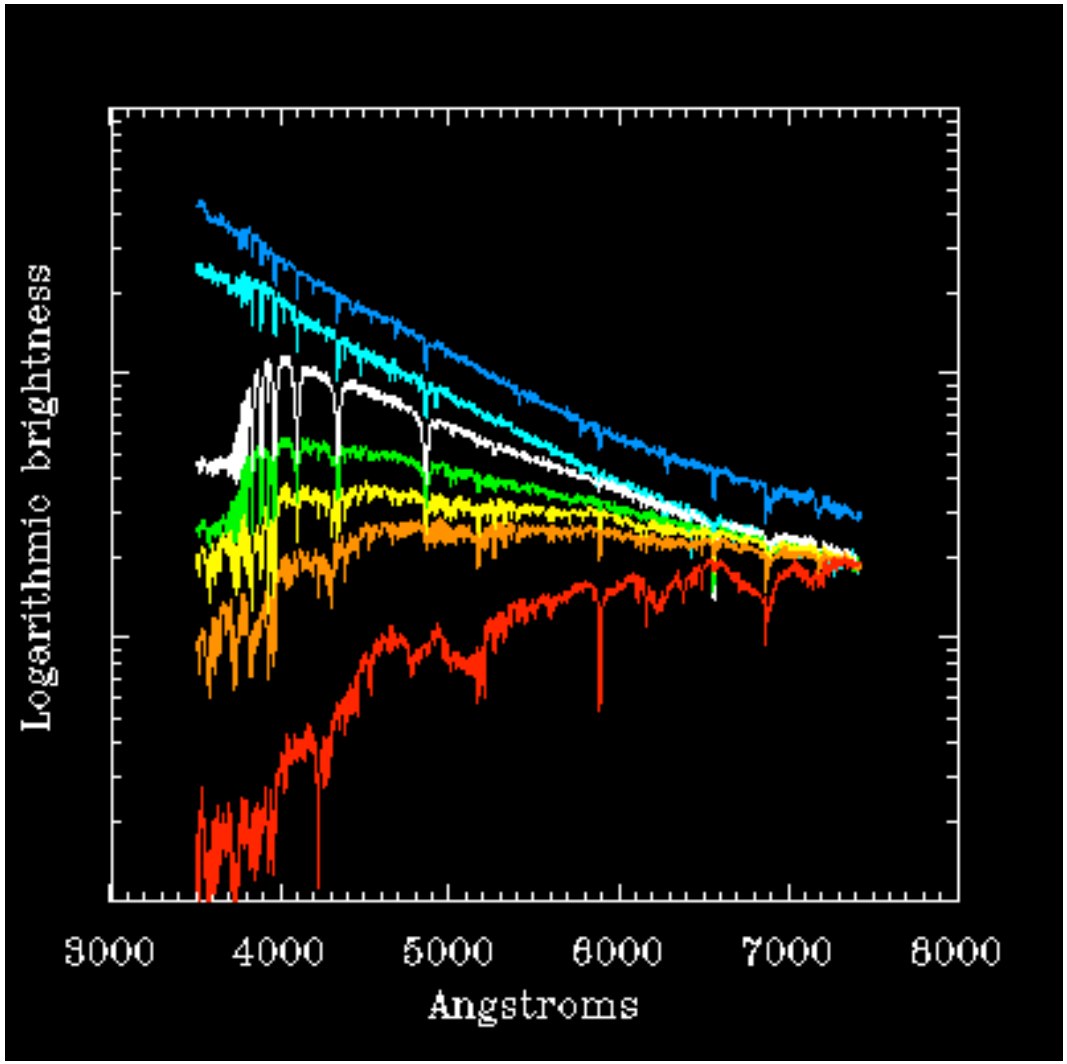

Stellar spectra I

O stars are the hottest, with temperatures from about 20,000K up to more than 100,000K. These stars have few absorption lines, generally due to helium. These stars burn out in a few million years.

- **B** stars have temperatures between about 10,000 and 20,000K. They are noticeably blue.
- **A** stars have strong absorption lines of Hydrogen. Temperatures are about 8000-10,000K. They appear white.
- **F** stars are slightly hotter than the Sun. Absorption lines of metals appear
- **G** stars have temperatures between 5000 and 6000K. They appear yellow. Our Sun is a G star and lives for 10 Gyr
- **K** stars appear orange. Temperatures are 3000-5000K.
- **M** stars are the coolest stars. They are so cool (2000-3000K) that molecules, including water, carbon monoxide, Vanadium Oxide and Titanium oxide are visible.

$$\text{Ages} \approx \frac{10\,\text{Gyr}}{(M/M_\odot)^3}$$

info: http://www.astro.sunysb.edu/fwalter/AST101/spt.html

- Most stars are called **main sequence stars** or **dwarfs**. These are stars which are burning Hydrogen stably. O dwarfs are about 50 times as massive as the Sun, and a million times as bright; M dwarfs may be as small as a tenth the mass of the sun and one ten-thousandth as bright. Stars which have used up their core hydrogen and are beginning to burn out expand into **subgiants**, **giants**, and **super giants**. Later they may become **white dwarfs**. These categories are called **luminosity classes**. Note that there is no such thing as a normal star.

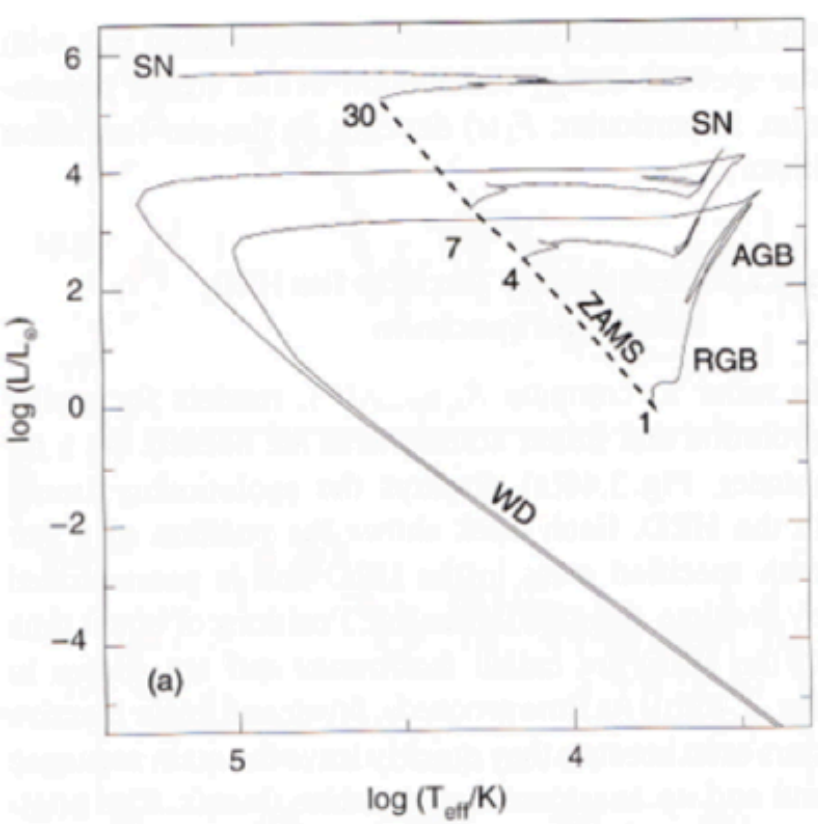

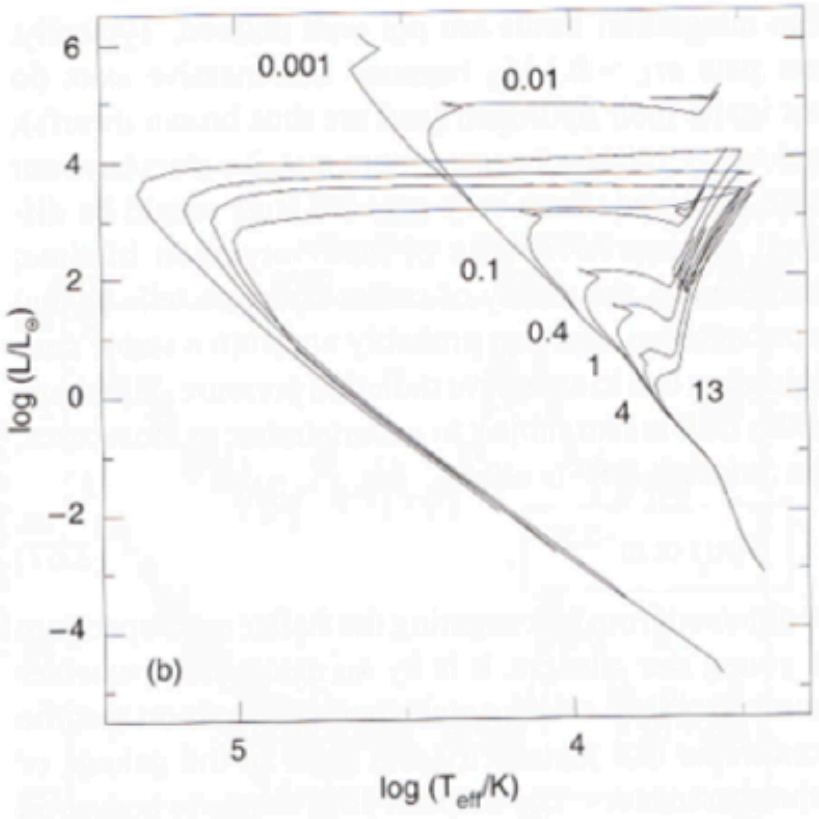

Fig. 3.46. a) Evolutionary tracks in the HRD for stars of different masses, as indicated by the numbers near the tracks (in units of $M_\odot$). The ZAMS (zero age main sequence) is the place of birth in the HRD; evolution moves stars away from the main sequence. Depending on the mass, they explode as a core-collapse SN (for $M \geq 8M_\odot$) or end as a white dwarf (WD). Prior to this, they move along the red giant branch (RGB) and the asymptotic giant branch (AGB). **b**) Isochrones at different times, indicated in units of 10^9 years. The upper main sequence is quickly depopulated by the rapid evolution of massive stars, whereas the red giant branch is populated over time

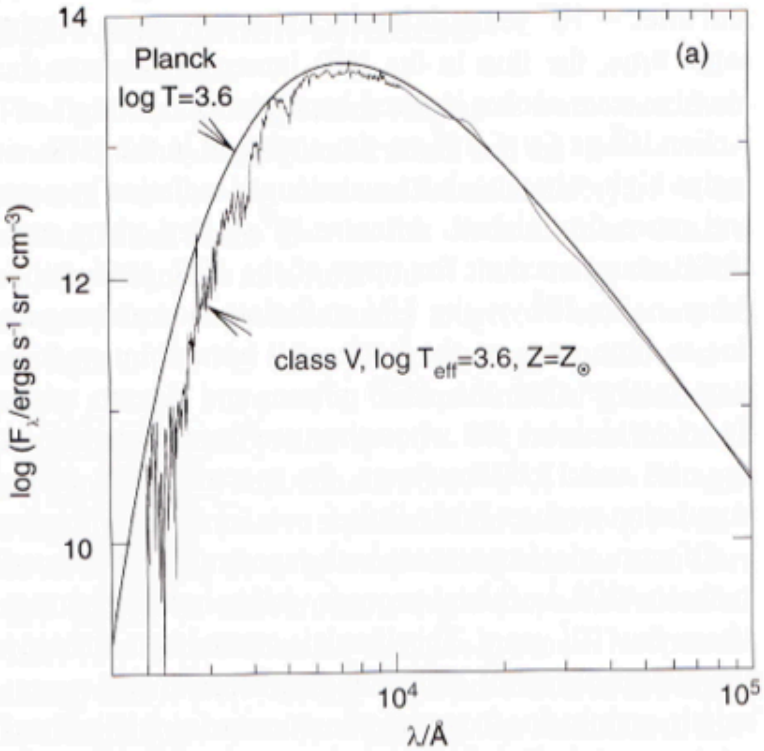

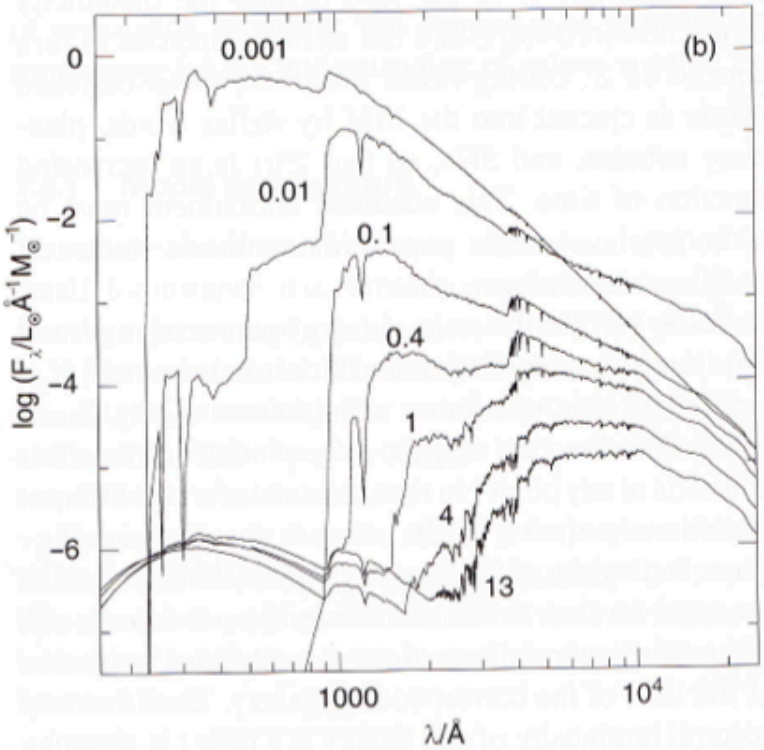

Fig. 3.47. **a**) Comparison of the spectrum of a main-sequence star with a blackbody spectrum of equal effective temperature. The opacity of the stellar atmosphere causes clear deviations from the Planck spectrum in the UV/optical. **b**) Spectrum of a stellar population with solar metallicity that was instantaneously born a time t ago; t is given in units of 10^9 years

Photometric and spectroscopic redshifts; spectral features

- Emission lines: photoionization of warm gas by hot O and B stars
- Blue spectra
  - young stars
  - spiral disks
- Red spectra
  - old stars
  - ellipticals, bulges
- Balmer break = 4000 Angstrom break
  - due to continuum absorption
- Lyman break
  - Absorption due to intervening neutral gas clouds
    - due to $n = 2 \rightarrow 1$ hydrogen transition at 121.6 (1+z) nm
    - and especially due to $n = \infty \rightarrow 1$ hydrogen transition at 91.2 (1+z) nm
  - Basis of the U-band dropout technique to find Lyman break galaxies

II. High redshift galaxies

- Lyman break galaxies (355-358)
- Photometric redshift (9.1.2)
- Deep fields (9.1.3)
- Starburst galaxies (9.2.1)
- Extremely red objects (9.2.2)
- Submm galaxies (9.2.3)
- Cosmic starformation rate history (9.5)
- Downsizing (9.6.4)

Lyman Break galaxies

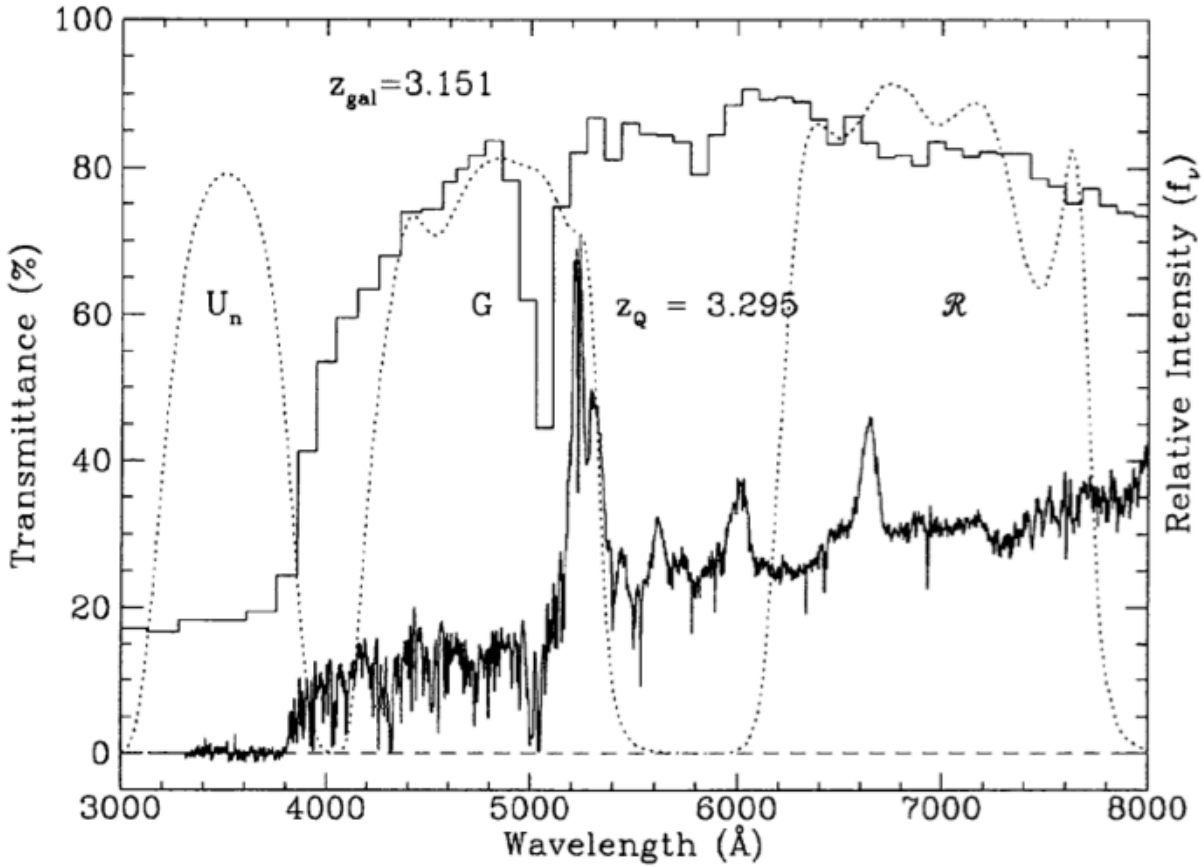

FIG. 1. Spectral energy distribution of a star-forming galaxy at $z=3.151$ from the population synthesis models by Bruzual & Charlot (1993); the example reproduced here is for a generic Im galaxy and assumes a Salpeter IMF. The broken lines show the transmission curves of the three broadband filters used in this work, chosen specifically to detect the Lyman break at 912 Å (U_n and G) and the relatively flat continuum longward of the break (G and $\mathscr{R}$). Also shown in the figure is the spectrum of the $z_{em}=3.295$ QSO Q2233+1310; an optically thick Lyman limit system at $z_{abs}=3.151$ produces the marked discontinuity near 3900 Å. Details of the QSO spectrum are given in Sec. *4.4*.

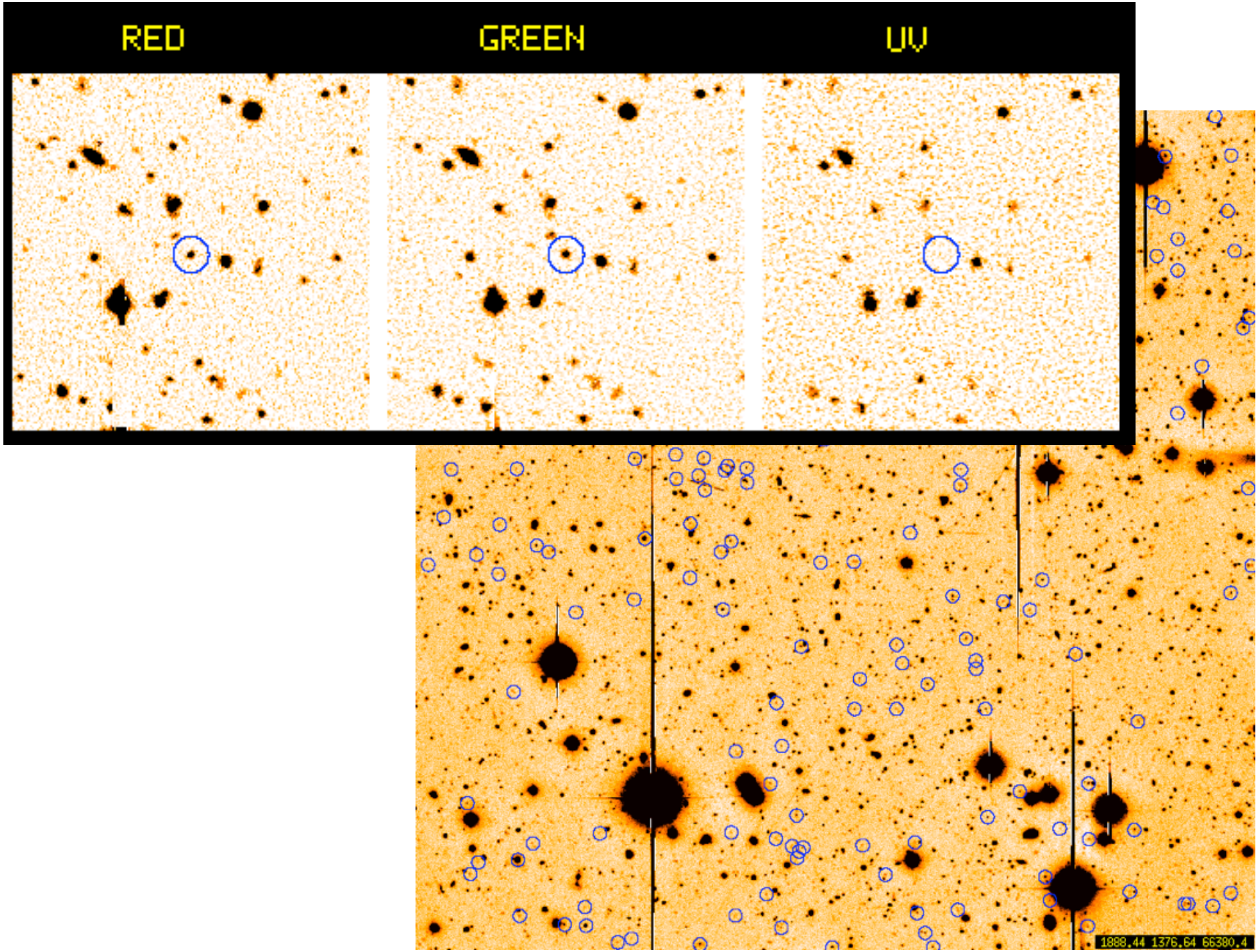
RED
GREEN
UV
1888.44 1376.64 66380.4

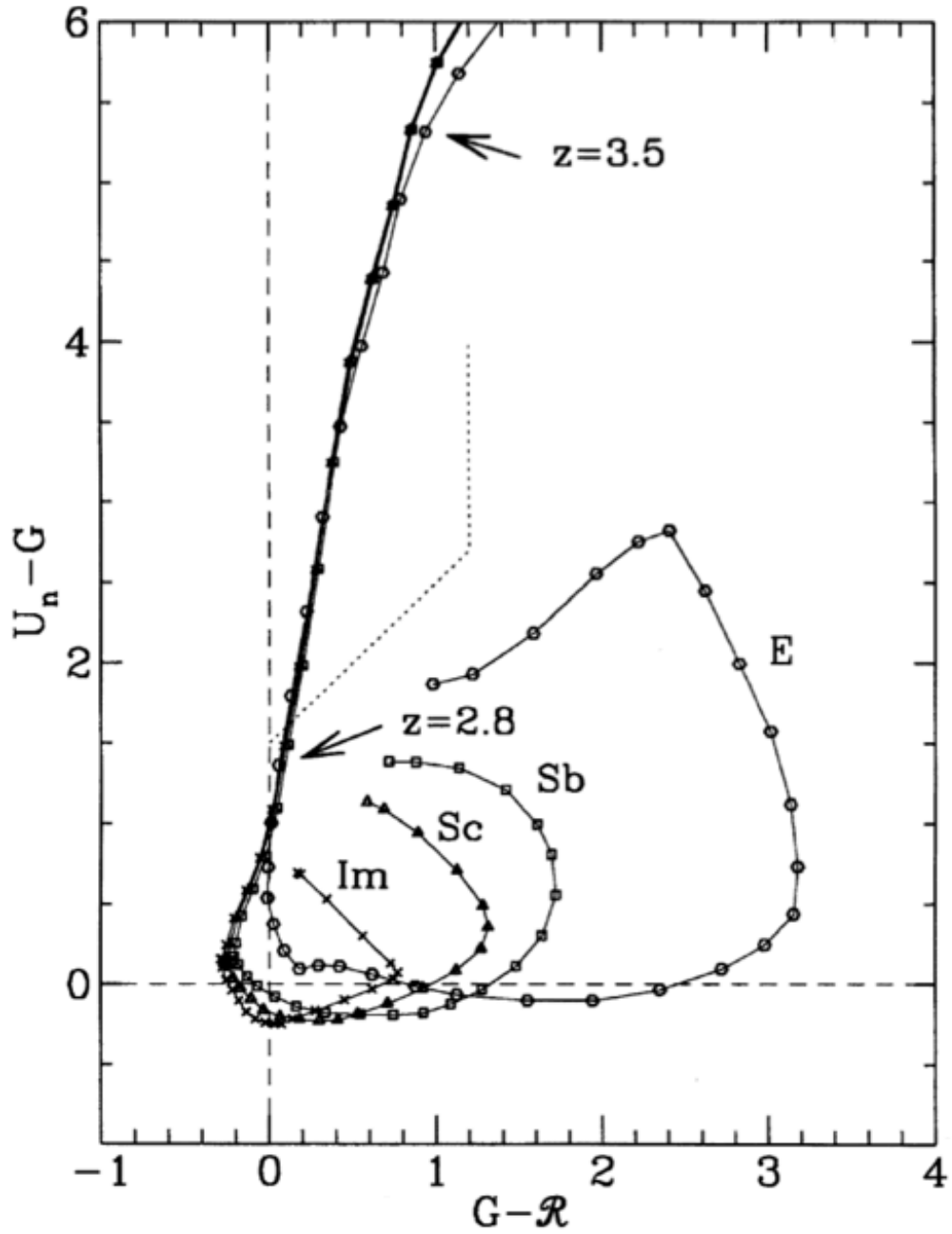

FIG. 2. Color evolution of galaxies of different spectroscopic type in the three passbands used in this work; points are plotted at redshift intervals $\Delta z = 0.1$ starting from $z = 0.0$. In producing the plot we have combined the spectral energy distributions by Bruzual & Charlot (1993) with Madau's (1995) statistical estimates of Lyman line and continuum blanketing by intervening gas. No allowance has been made for Lyman absorption by the interstellar medium of the galaxies themselves. The dotted line indicates the locus of points which we expect to be occupied by high-redshift galaxies ($z \gtrsim 3$).

Photometric redshifts

- Spectroscopic redshift
  - location emission or absorption lines
- Photometric redshift
  - fit galaxy template to estimate redshifts
  - generally okay, but catastrophic outliers

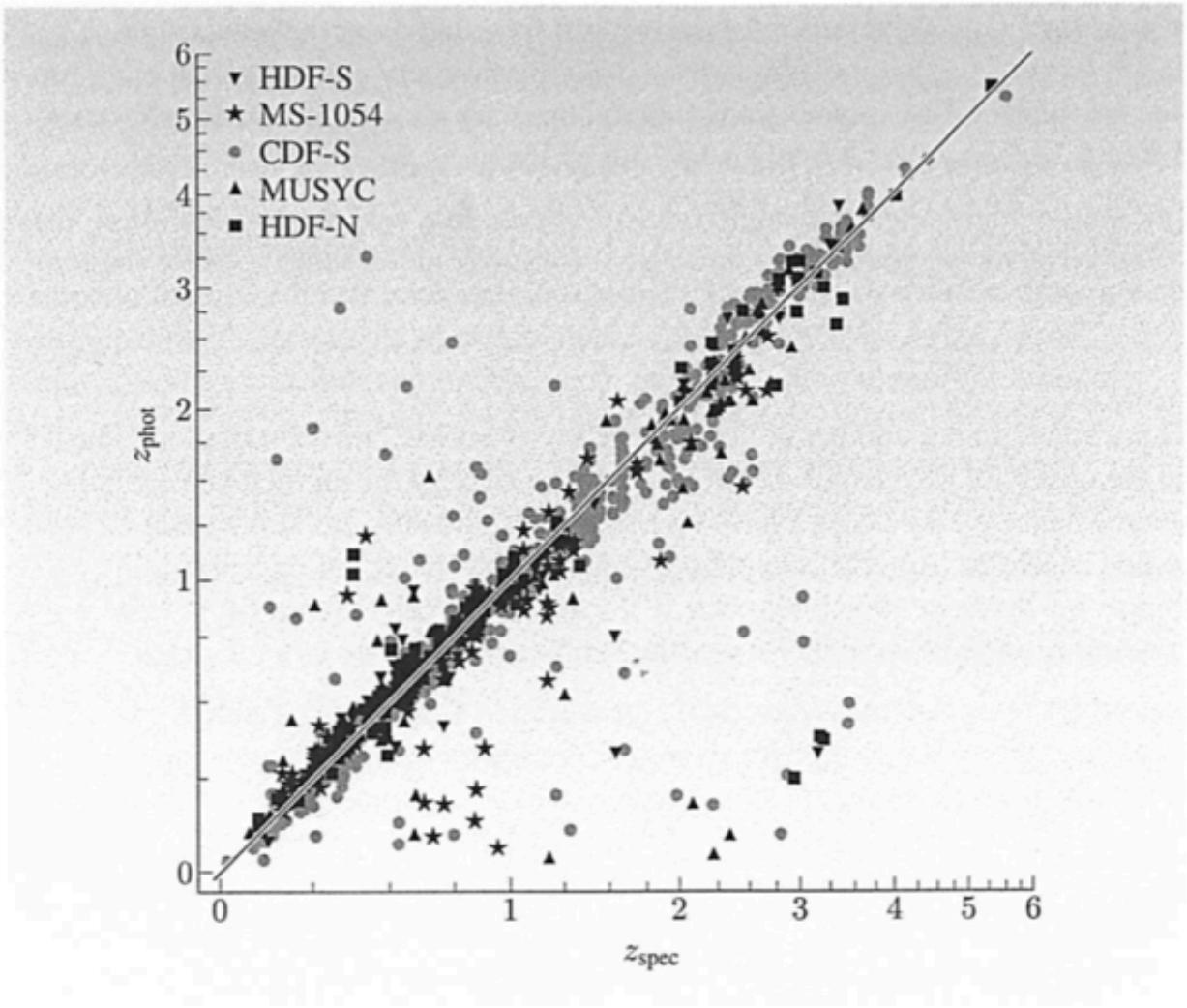

Figure 4.9 A comparison of photometric redshift estimates with spectroscopic redshifts (which have much higher precision). Note that while the technique works for most objects, there are some strongly outlying points known as 'catastrophic' failures. Five survey data sets are used and are marked in different symbols.

SS p. 134

Deep field survey

- Many types of galaxies
  - dropouts galaxies
  - extremely red galaxies
  - Lyman alpha galaxies
- Main results
  - Increased merger rate
  - Higher fraction of irregular galaxies
  - Distant massive galaxies can be small (~1 kpc)
  - Cosmic star formation history

Starburst galaxies

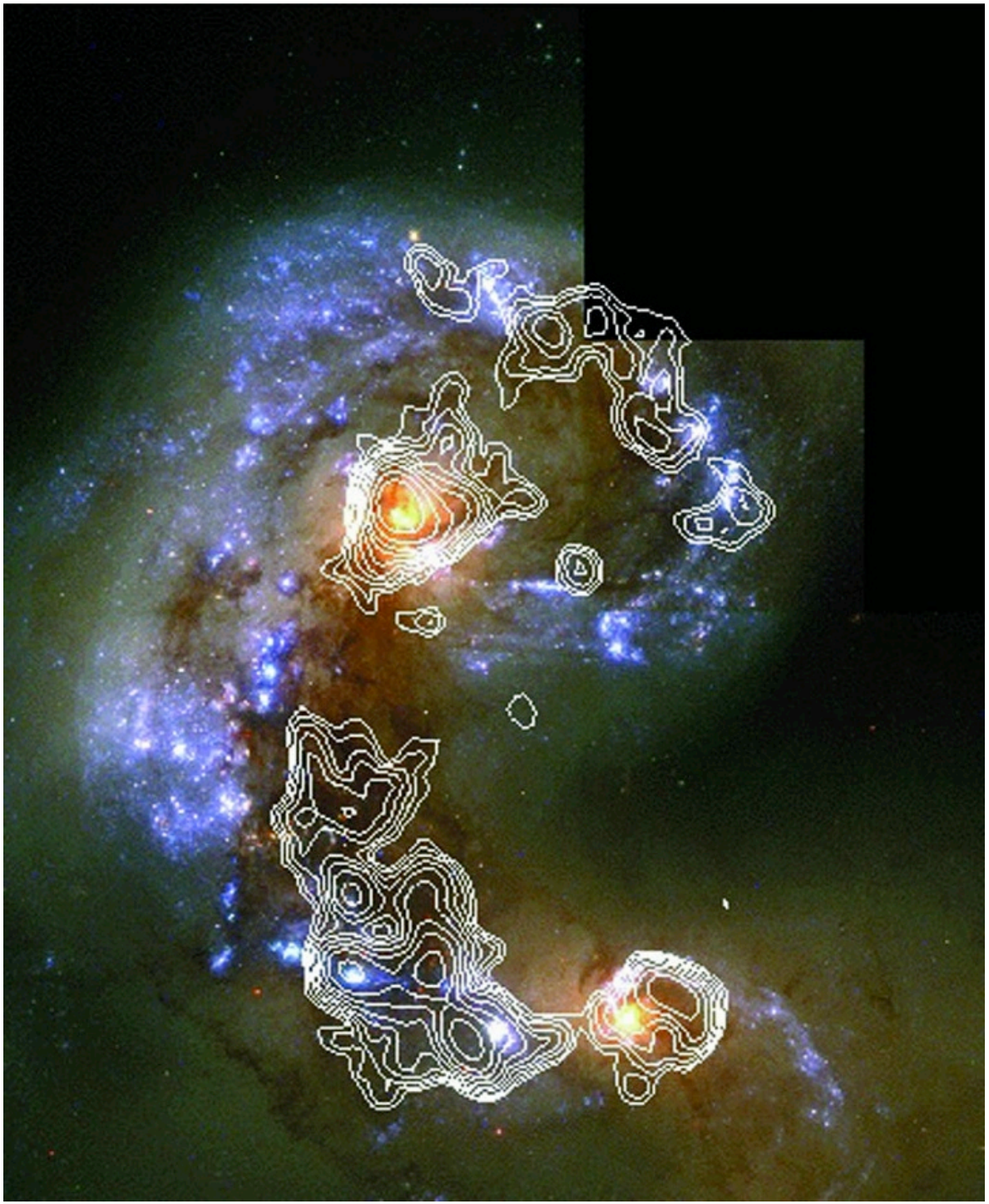

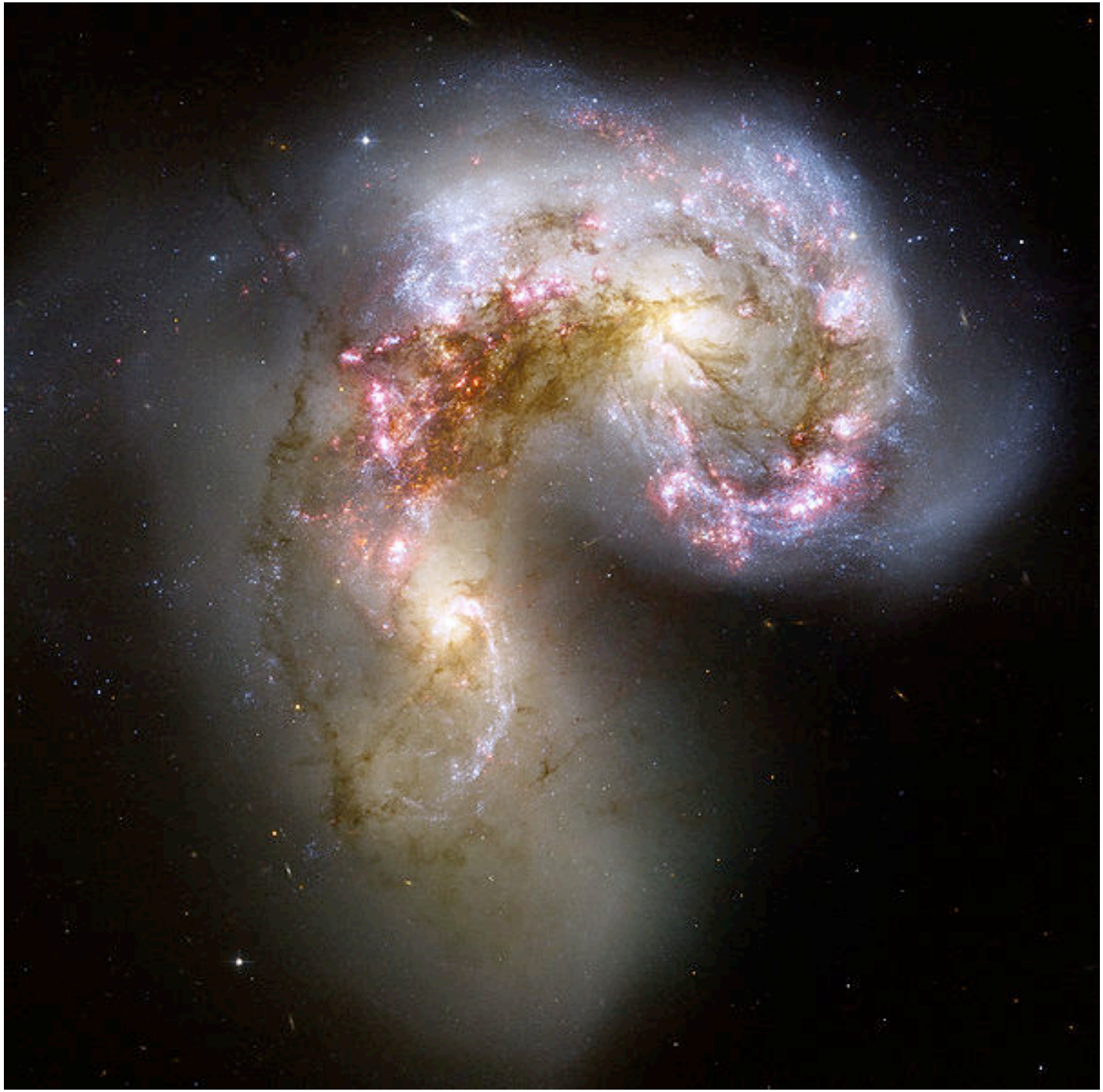

Extremely red galaxies

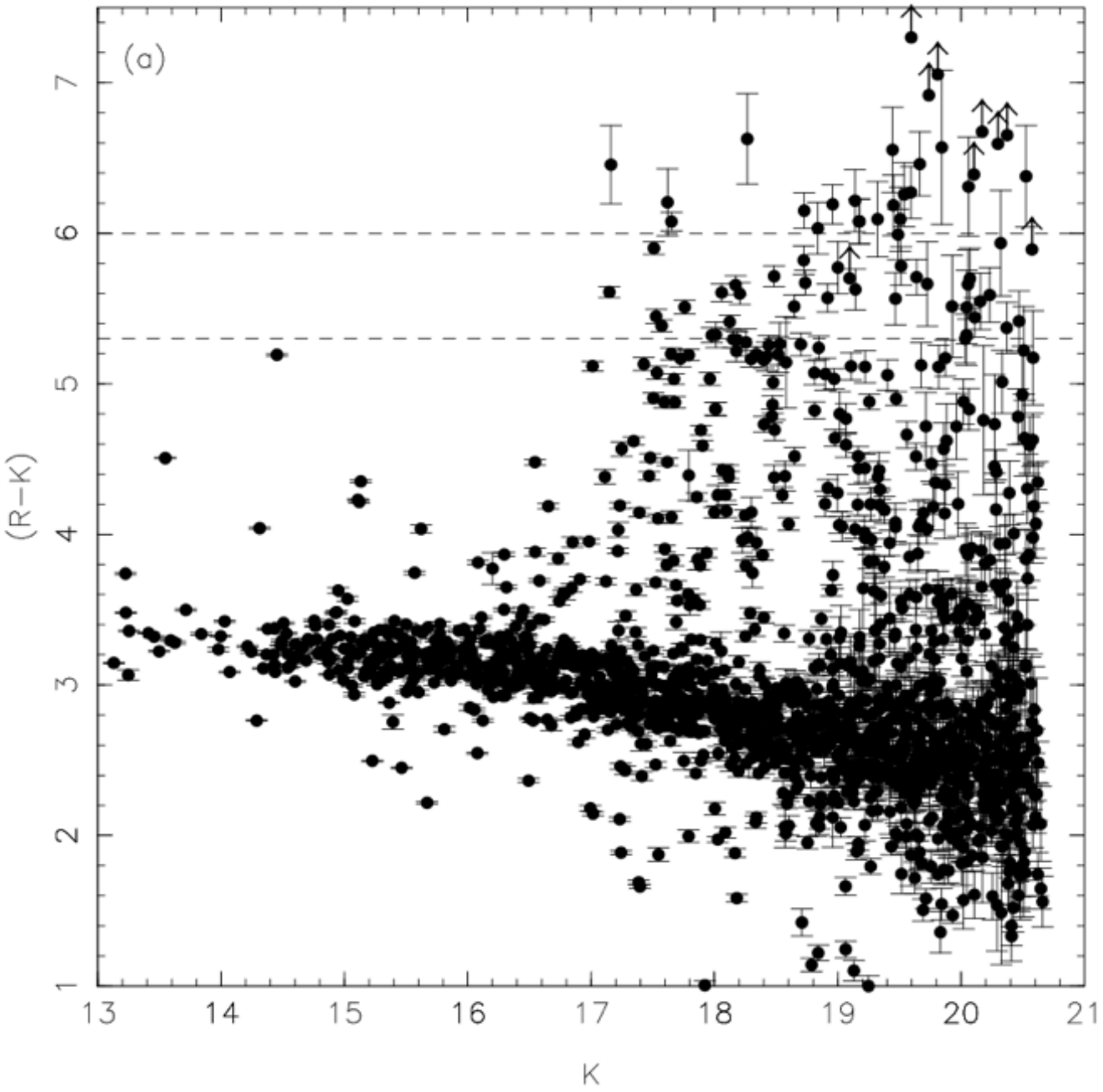
(a)
(R−K)
K
1
2
3
4
5
6
7
13
14
15
16
17
18
19
20
21

Submillimeter galaxies

- IRAS (1983) mapped 98 % of the sky at 12, 25, 60 and 100 micron.
- surprise: many galaxies with L~ 10^12 Mo, 10-100 more than our own galaxy
  - luminous IR galaxies L = 10^11-10^12 Mo
  - ultra-luminous IR galaxies: L = 10^12-10^13 Mo
  - hyper-luminous: L > 10^13 Mo
- HST imaging: major galaxy galaxy merging systems

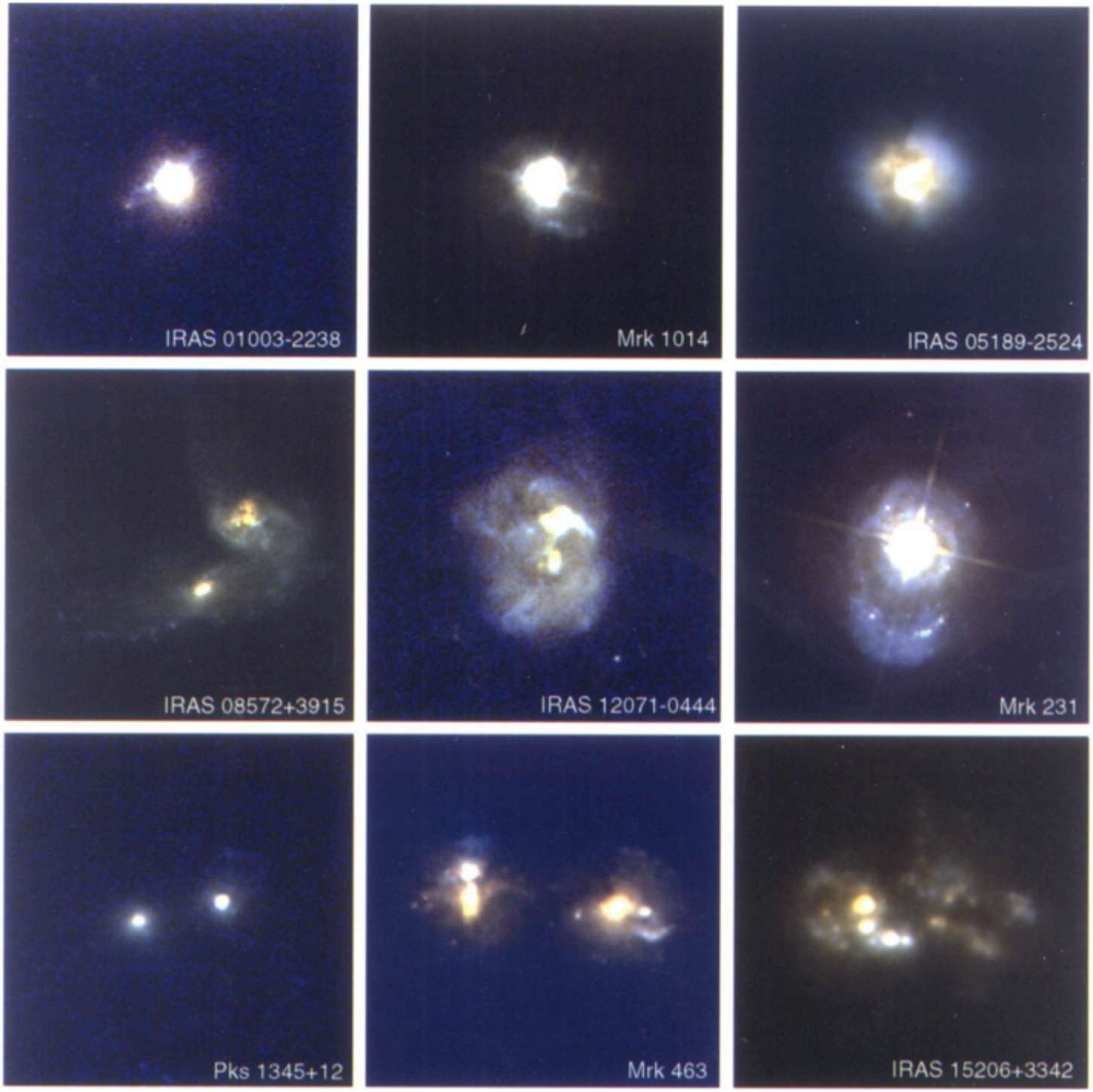
IRAS 01003-2238
Mrk 1014
IRAS 05189-2524
IRAS 08572+3915
IRAS 12071-0444
Mrk 231
Pks 1345+12
Mrk 463
IRAS 15206+3342

Submm galaxies and K-corrections

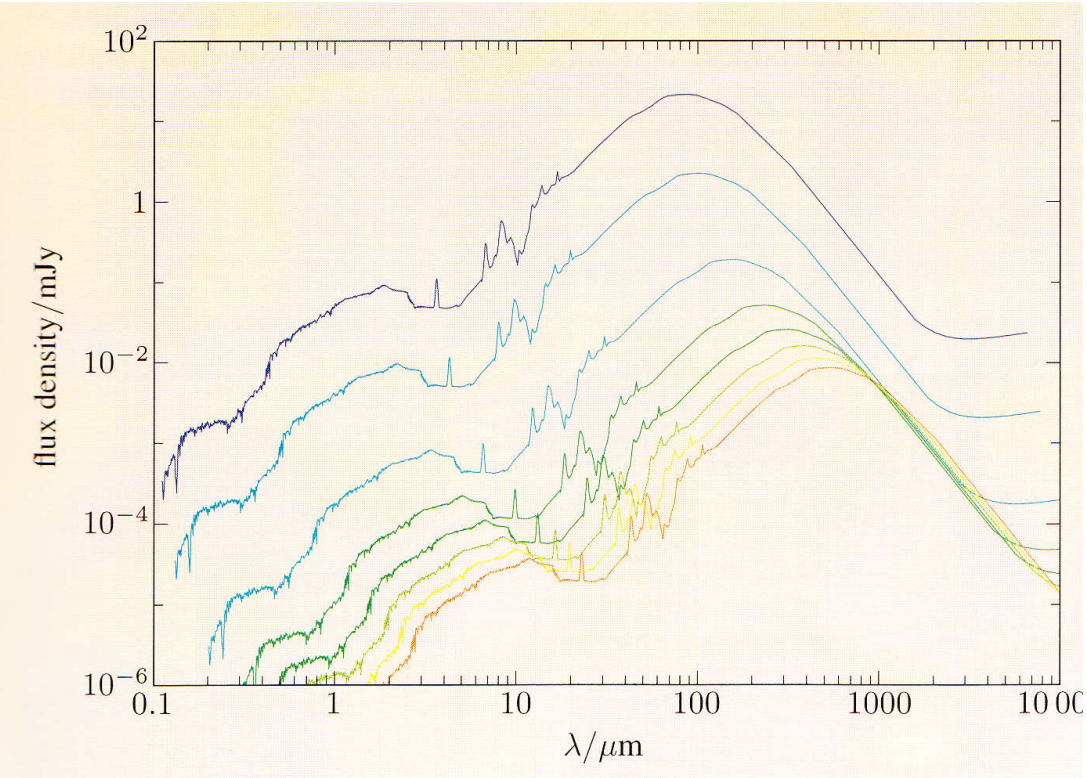

Spectral energy distribution of star forming galaxy M82, as it would appear at z=0.1, 0.3, 1, 2, 3, 4, 5 and 6

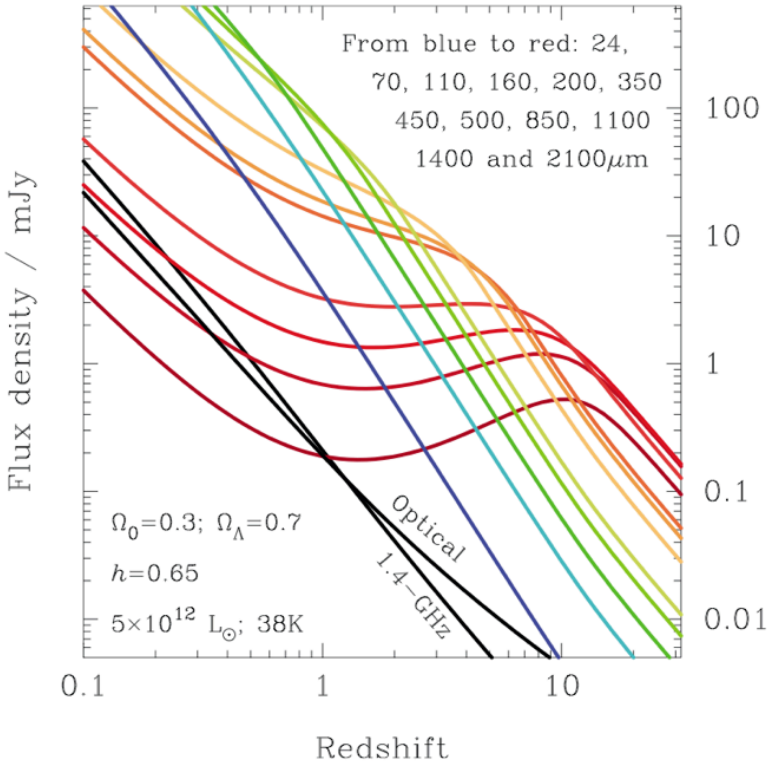

Negative K-correction: sub-mm galaxies get brighter at larger distances due to the steep Rayleigh-Jeans slope of the thermal dust emission

Cameras operating at submm-mm wavelengths

James Clerk Maxwell Telescope (JCMT) in Hawaii

Submm Common User Bolometer Array (SCUBA)

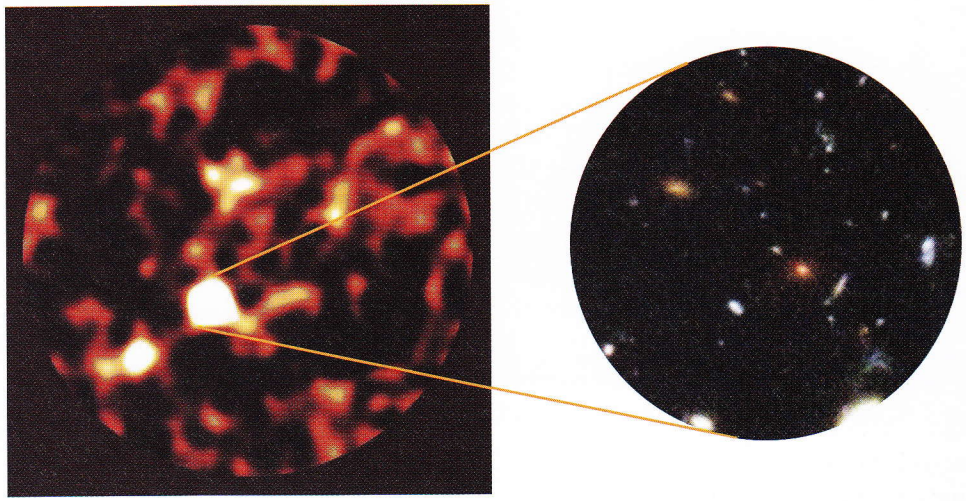

Figure 5.5 The 850 μm image of the Hubble Deep Field North. This image has a radius of 100 arcseconds. The zoom shows the corresponding Hubble Space Telescope data in the region of the brightest SMG.

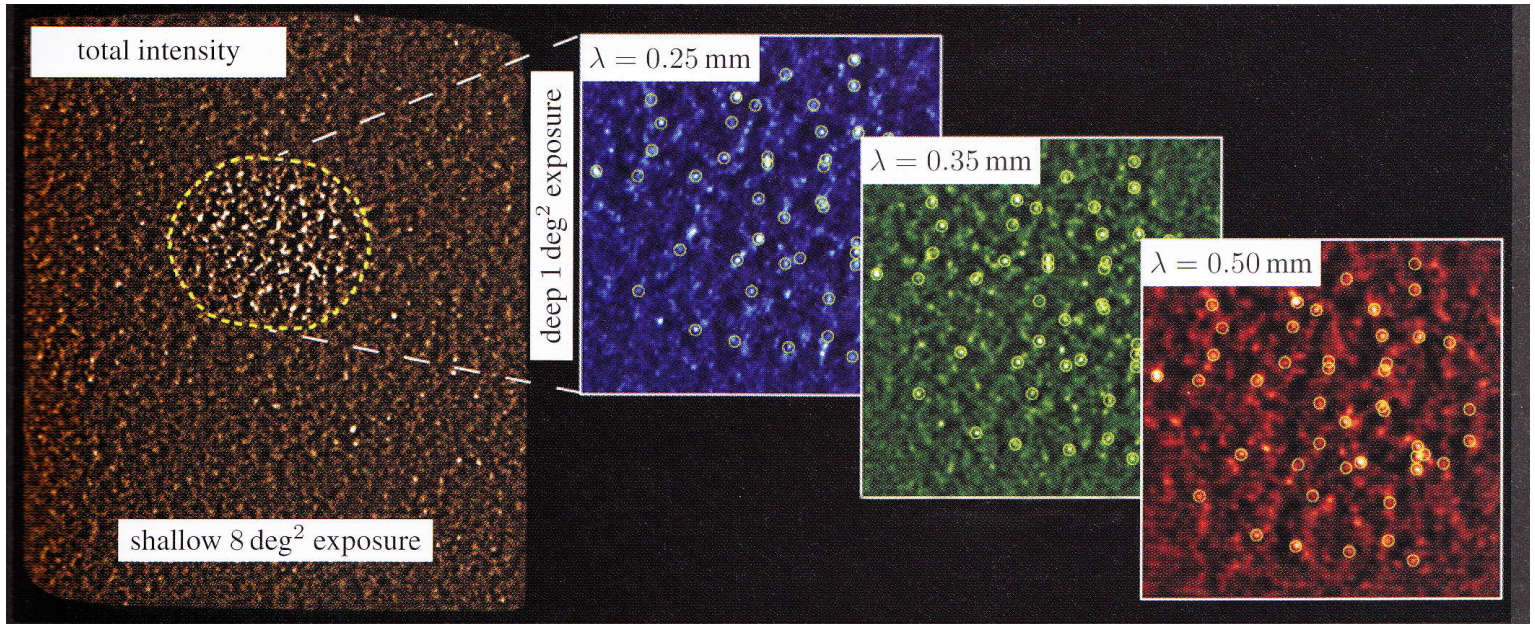

Figure 5.6 Submm-wave maps of the Chandra Deep Field South region from the BLAST mission. For reference, the same features have been circled in each of the images. Total intensity = sum of the three wavelengths.

Sub-mm surveys

- Small to large areas
  - scuba, blast -> Herschel
  - diffraction limit l/D gives not very high resolution -> identification difficult
  - Detailed studies: ALMA
- Sources
  - Properties
    - copious amount of dust, optical light largely extinguished
    - star formation rates ~ 1000 M/yr
    - median z =2.2
  - Interpretation
    - a significant fraction of the stars of a future massive ellipticals is being formed

Cosmic starformation history

Measuring star formation rates

1. UV light emitted by O and B stars
2. Strengths of emission lines like Ly-alpha, H-alpha, [OII], which are ionised by UV light from O and B stars
   - issues
     - traces un-obscured regions
     - (redshifted) lines need to be in observing window
3. Dust emission
   - O and B stars heat up dust
4. Radio emission
   - supernova accelerate charged particles that radiate synchrotron emission while spiraling around the galactic magnetic field lines
   - no dust obscuration

Radio-IR correlation

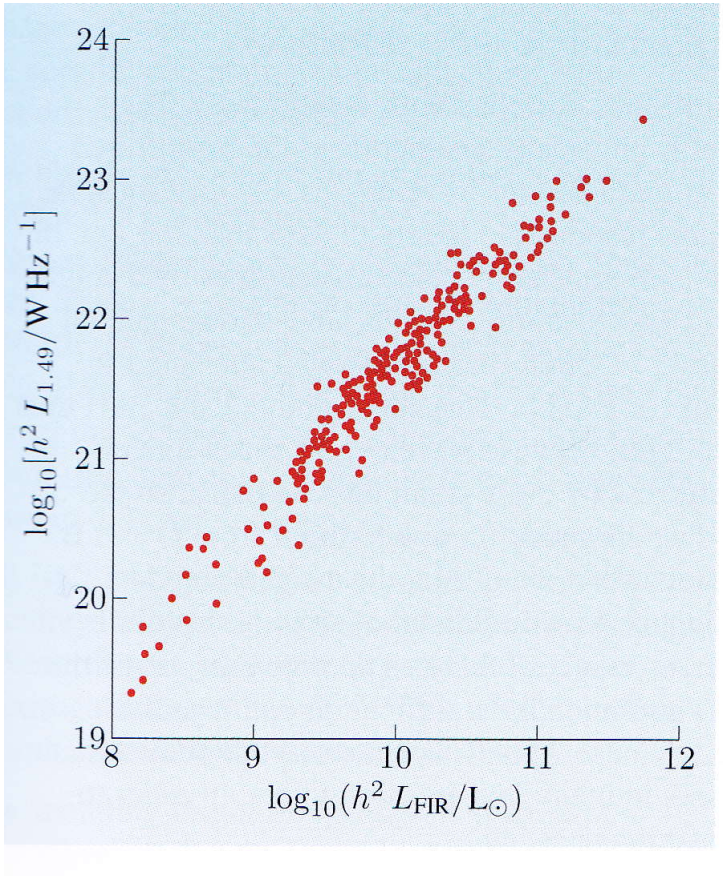

Figure 5.13 The correlation between far-infrared and radio (1.49 GHz) luminosities of star-forming galaxies. Galaxies with active nuclei have been excluded from this plot.

- over 4 orders of magnitude
- not well understood why so tight

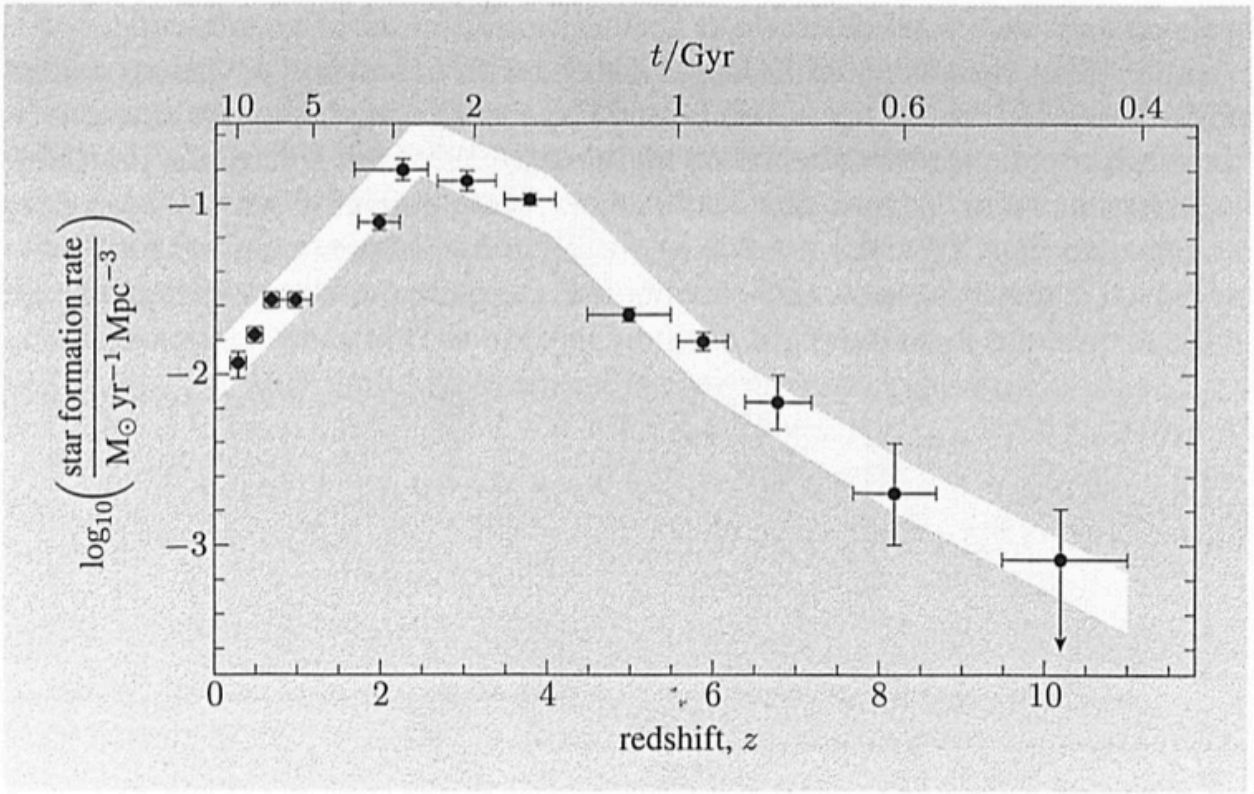

Figure 4.24 The cosmic star formation history (also known as the Madau diagram) derived from rest-frame ultraviolet luminosities of galaxies. The data have had a correction for dust extinction applied.

6. Cosmic star formation history and stellar mass assembly

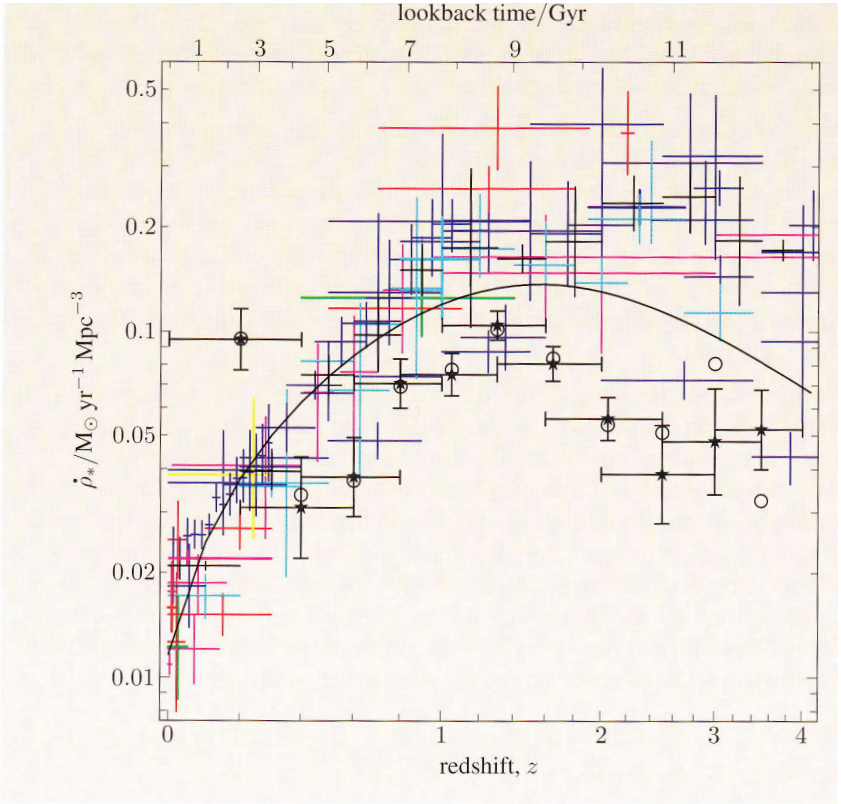

Figure 5.17 The comoving star formation density history of the Universe, derived from mid-infrared luminosities (blue error bars) and submm luminosities (magenta error bars). These estimates have been averaged together to make the black error bars. The error bars with filled stars and the open circles show the result of differentiating Figure 5.16, and are substantially lower.

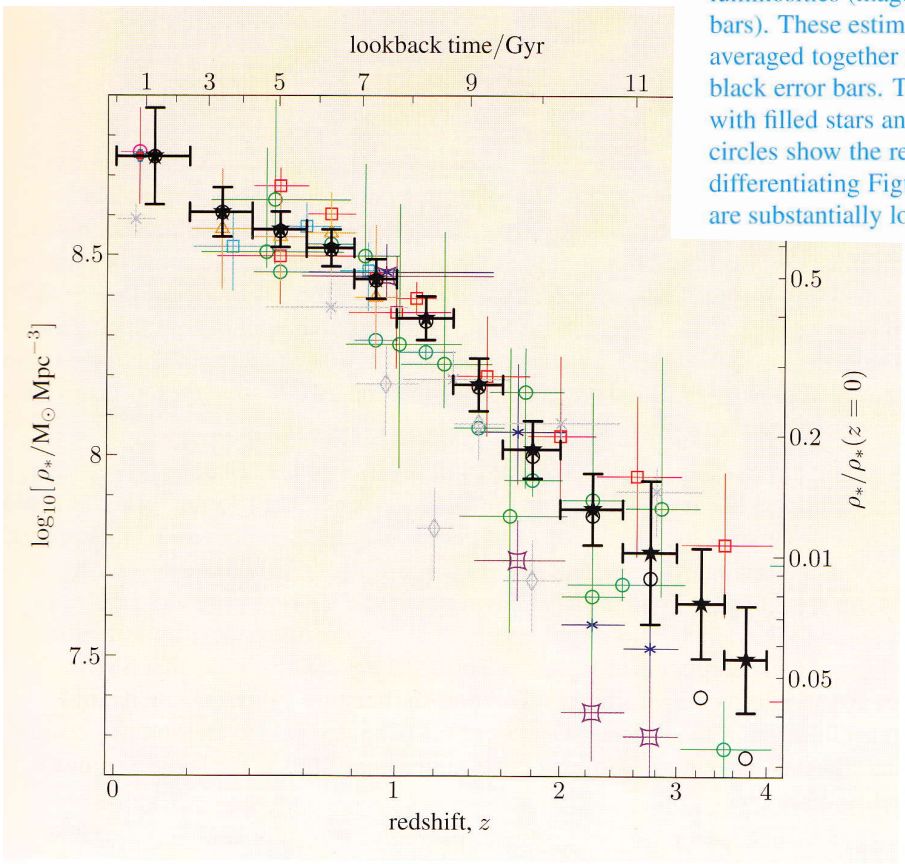

Figure 5.16 The stellar mass density of the Universe as a function of time and of redshift. A compilation of earlier estimates is shown in coloured symbols, while the most precise determination so far is shown in black symbols. Open circles show the direct measurements, while filled stars incorporate an additional correction for galaxies below the flux limits of the data.

Not fully consistent: problems with dust extinction corrections, AGN contribution, mass estimates, IMF?

Downsizing

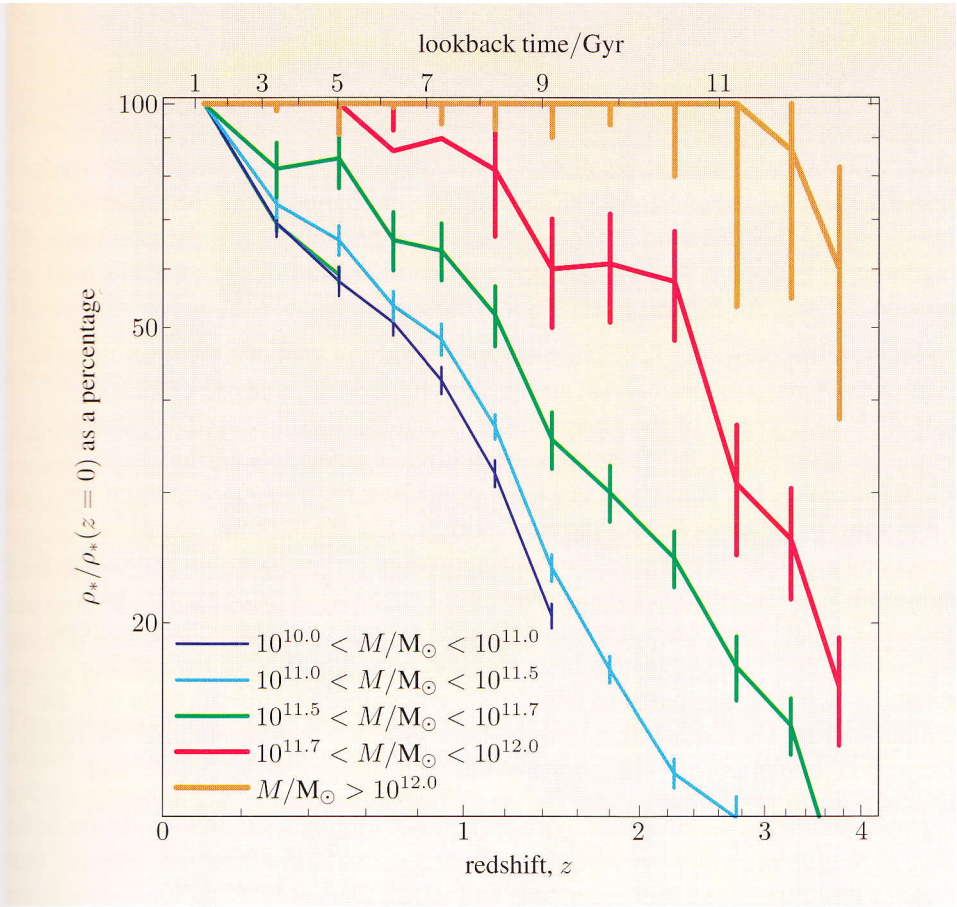

Figure 5.18 The fraction of the present-day assembled stellar mass, for a variety of galaxy masses. Note that the most massive galaxies formed their stars earlier in the history of the Universe.

massive galaxies formed earlier then less massive galaxies

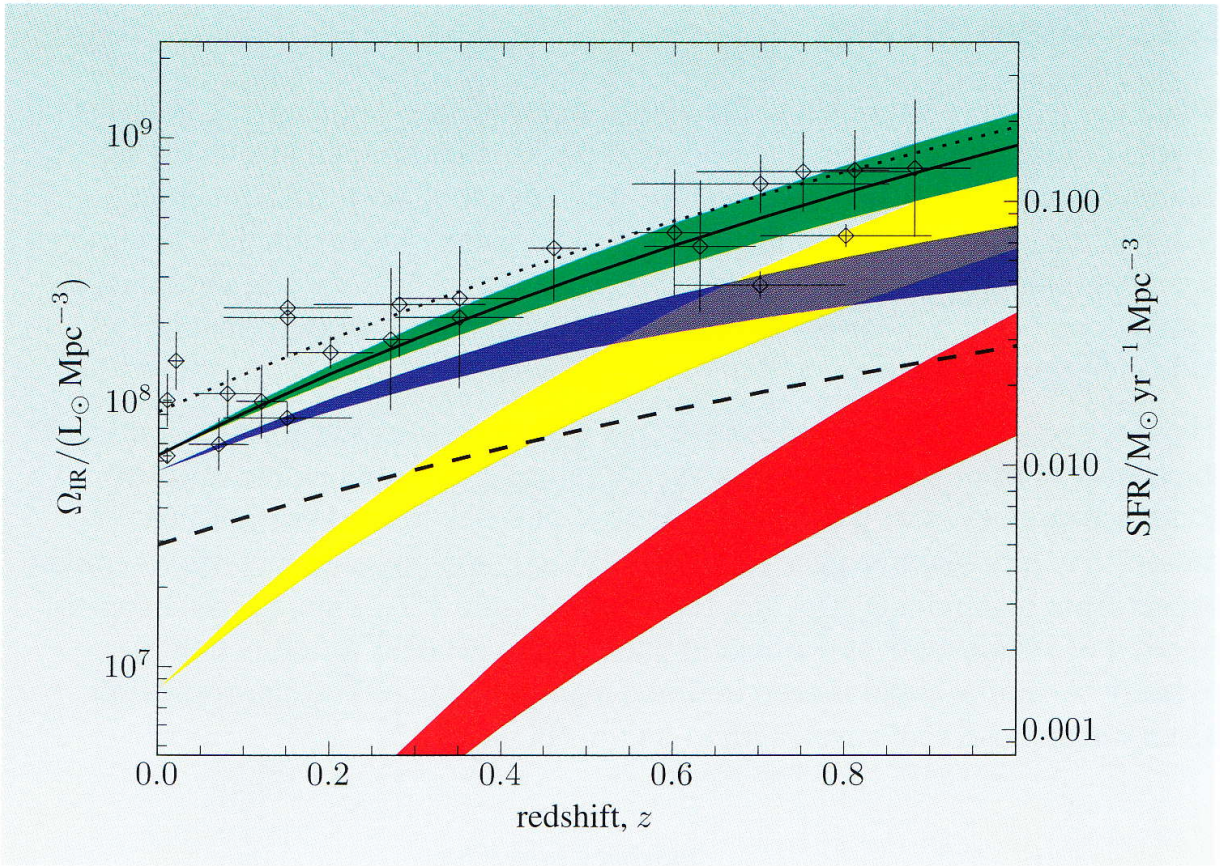

Figure 5.19 The cosmic star formation history for all galaxies (green), for $< 10^{11}\,L_\odot$ galaxies (blue), and for galaxies with $> 10^{11}\,L_\odot$ (yellow) and $> 10^{12}\,L_\odot$ (red). The contribution from higher-luminosity galaxies evolves more quickly, making it negligible in the present-day Universe but important by $z = 1$.

13. Home work

- Locate data in Table 3 from Rieke G. H. et al. 2009, ApJ, 692, 556
- Plot for two galaxies from this table their spectra.
- What are the star formation rates for these two galaxies from the literature?
- How does total flux scale with redshift (see Schneider eq. 4.46) ? Illustrate this with a plot using recent parameters for the cosmological constant. Hint: use again IDL routines as given in http://idlastro.gsfc.nasa.gov/ or use http://www.astro.ucla.edu/~wright/CosmoCalc.html
- Plot flux density with redshift for an object that has a flux density of 1 Jy at z=1. Note that the flux density is flux per (observed) frequency interval.
- Plot for the two galaxies from Rieke et al their flux density at 1.4 and 350 GHz as a function of redshift.
  - explain the different behavior for the two different frequencies
- Taking these redshifted spectra, what are the flux densities at 1.4 and 350 GHz.
- Scaling with the star formation rates of these galaxies, what what are the flux densities at 1.4 and 350 GHz for galaxy with a star formation rate of 100 M/yr
- Compare this these numbers to the result of Carilli and Yun, 1999 ApJ, 513, 13, page L16
  - Why are the three estimates somewhat different?